JCI insight

Loss of *Glp2r* signaling activates hepatic stellate cells and exacerbates diet-induced steatohepatitis in mice

Shai Fuchs, … , Dianne Matthews, Daniel J. Drucker

JCI Insight. 2020. https://doi.org/10.1172/jci.insight.136907.

Research In-Press Preview Endocrinology Metabolism

Graphical abstract

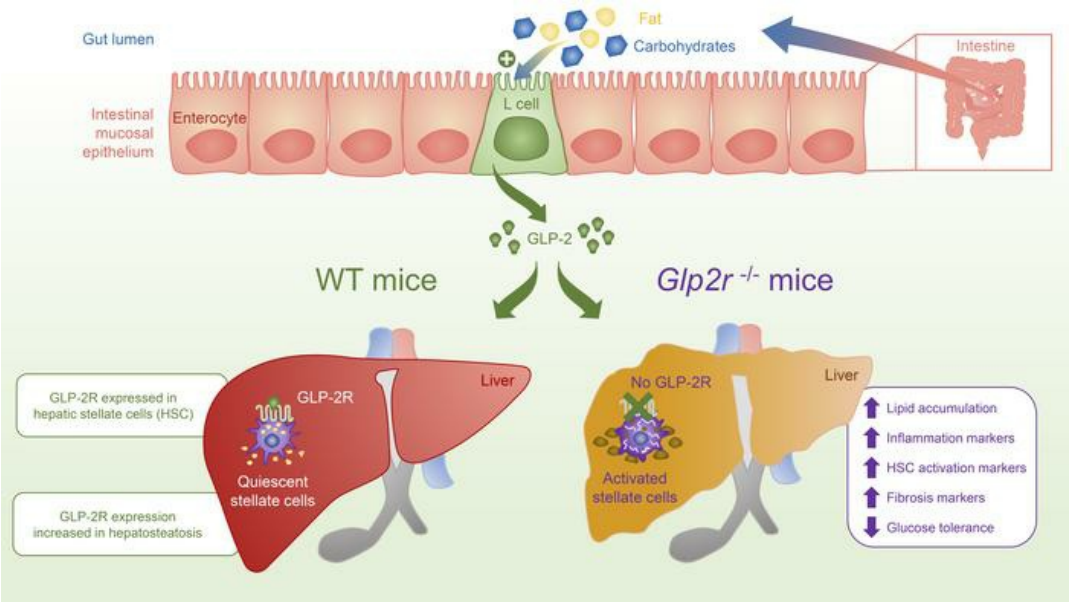

Loss of *Glp2r* signaling activates hepatic stellate cells and exacerbates diet-induced steatohepatitis in mice

Shai Fuchs[1,2] Bernardo Yusta[1] Laurie L Baggio[1] Elodie M Varin[1]; Dianne Matthews[1] Daniel J Drucker[1,3]

[1]Lunenfeld Tanenbaum Research Institute, Mount Sinai Hospital, Toronto, ON M5G1X5 Canada

[2]The Hospital for Sick Children, [3]Department of Medicine, University of Toronto, Toronto ON M5G1X8 Canada

Address correspondence to:

Dr. Daniel J. Drucker

LTRI, Mt. Sinai Hospital

600 University Avenue Toronto ON M5G1X5

drucker@lunenfeld.ca

Tel: +1-416-361-2661

Daniel J. Drucker is the Lead Contact and takes primary responsibility for the data shown in this manuscript

Duality of Interest: The pharmaceutical development of GLP-2 is the subject of a license agreement between DJD, Toronto General Hospital, University of Toronto, and Shire-Takeda Inc. This work was supported in part by an investigator-initiated operating grant from Shire-Takeda Inc. to Mt. Sinai Hospital for work in the Ducker laboratory. None of the other authors have any conflict of interest.

Summary

A GLP-2 analogue is used in individuals with intestinal failure at risk for liver disease, yet the hepatic actions of GLP-2 are not understood. Treatment of high fat diet (HFD)-fed mice with GLP-2 did not modify development of hepatosteatosis or hepatic inflammation. In contrast, *Glp2r*$^{-/-}$ mice exhibited increased hepatic lipid accumulation, deterioration in glucose tolerance, and upregulation of biomarkers of hepatic inflammation. Both mouse and human liver expressed the canonical GLP-2R, and hepatic *Glp2r* expression was upregulated in mice with hepatosteatosis. Cell fractionation localized the *Glp2r* to hepatic stellate cells (HSC), and markers of HSC activation and fibrosis were increased in livers from *Glp2r*$^{-/-}$ mice. Moreover, GLP-2 directly modulated gene expression in isolated HSCs ex vivo. Taken together, these findings define an essential role for the GLP-2R in hepatic adaptation to nutrient excess and unveil a gut hormone-HSC axis, linking GLP-2R signaling to control of hepatic stellate cell activation.

Key words: gut hormones, G protein coupled receptor, glucagon, GLP-2, liver, intestine, inflammation, hepatic stellate cells, steatohepatitis

Introduction

Glucagon-like peptide-2 (GLP-2) is a 33-amino acid proglucagon-derived peptide that is secreted, together with GLP-1, from the intestinal enteroendocrine L-cell (1). GLP-2 is continuously secreted at low basal levels in the fasting or interprandial state, and circulating levels rise briskly within minutes of food ingestion (2). GLP-2 exerts proliferative and cytoprotective actions in the small bowel, resulting in the expansion of the mucosal surface area, and enhanced nutrient absorption (3, 4). Sustained augmentation of GLP-2R signaling with a degradation-resistant GLP-2 analogue, teduglutide, reduces the requirement for parenteral nutrition (PN) in human subjects with short-bowel syndrome (SBS) (5), and is approved for the therapy of adults and children with PN-dependent SBS (6).

Although the actions of GLP-2 are predominantly localized to the gut (7), the extra-intestinal expression of the GLP-2R raises important questions surrounding the safety of therapy with GLP-2R agonists, and potential actions of teduglutide beyond the gastrointestinal tract. For example, we recently detected robust expression of the GLP-2R in gallbladder, and demonstrated that administration of teduglutide markedly inhibits gallbladder emptying in mice (8). These findings, subsequently extended to human studies, are consistent with reports of increased numbers of gallbladder-related adverse events associated with teduglutide therapy (9).

A full length GLP-2 receptor (GLP-2R) mRNA transcript has also been identified in murine liver, albeit at levels much lower than in the jejunum (10). The GLP-2R was localized to hepatocytes (11), however GLP-2R mRNA transcripts were not identified within hepatocytes profiled by single-cell RNA Sequencing (scRNA-seq) (12). Moreover, the biological actions of GLP-2 on the liver are conflicting, with some preclinical studies demonstrating a detrimental effect on hepatic steatosis (13), whereas other reports highlight a hepatoprotective role for GLP-2, characterized by a reduction in markers of systemic and hepatic inflammation (14). The frequent development of hepatic steatosis in PN-dependent subjects with SBS, associated in some subjects with progression to hepatic failure and liver transplantation, highlights the importance of understanding the liver as a target of GLP-2 action (15, 16).

To resolve the hepatic actions of GLP-2, we have now studied GLP-2 action in high fat, high fructose, high cholesterol (HFHC)-fed wildtype mice, and simultaneously examined the hepatic phenotype of *Glp2r*$^{-/-}$ mice. Our findings demonstrate that expression of the hepatic *Glp2r* is induced following HFD feeding; however, sustained GLP-2R agonism has little impact on development of hepatic steatosis. In contrast, loss of the GLP-2R increases steatosis and biomarkers of hepatic inflammation. Furthermore, we localize a functional GLP-2R to hepatic stellate cells, and demonstrate increased markers of stellate cell activation in *Glp2r*$^{-/-}$ mice. Collectively, these findings reveal a prandial signal transduction pathway linking gut-derived GLP-2 to the control of hepatic stellate cell activity, with implications for understanding GLP-2 action in the context of nutrition-associated hepatocellular injury.

Results

GLP-2 does not alter the metabolic and inflammatory sequelae of HFHC feeding.

Previous studies of metabolic and hepatic health in HFD-fed mice and rats treated with GLP-2 have yielded conflicting results (13, 17). To study the effect of GLP-2 in the setting of energy excess, we administered GLP-2 to mice on 1) a HFHC diet or 2) a 10% fat control diet (CD) matched for other macronutrient sources. On week 15, (Figure 1A), mice were randomly allocated to treatment with either the long acting GLP-2 analogue h[Gly2]GLP-2, identical to teduglutide, hereafter referred to as GLP-2, or saline, for 11 days (Figure 1A). Body and liver weight was increased by the HFHC diet, but not different in GLP-2-treated mice (Figure 1B and Supplemental Figure 1A). GLP-2 increased small bowel length, total intestinal weight, and weight per cm as well as gallbladder volume (Supplemental Figure 1B,C). Intraperitoneal glucose tolerance and plasma lipid profiles (LDL, HDL, total cholesterol and triglyceride (TG)) were unaffected by GLP-2 treatment (Figures 1C-E). Hepatic Oil Red O staining (Figure 1F) and hepatic cholesterol and TG content (Figure 1G) were increased after exposure to HFHC diet, but not different in GLP-2-treated mice. Levels of hepatic mRNA transcripts encoding proteins important for lipid metabolic pathways were frequently modulated by diet, but not altered by GLP-2 treatment (Figure 1H).

Plasma alanine transferase (ALT) levels were higher (Figure 2A), and hepatic and plasma levels of KC/GRO, TNFα, and IL-10 were elevated in HFHC-fed mice, however none of the hepatic or plasma cytokines measured, including IL-1β, IFN-γ, IL-6 and IL-5, were different in GLP-2-treated mice (Figure 2B, Supplemental Figure 1D). Similarly, hepatic mRNA transcripts corresponding to markers of inflammation and fibrosis were not different after GLP-2 administration (Figure 2C). Thus, in HFHC-diet induced steatohepatitis, GLP-2 treatment did not impair indices of glucose and lipid metabolism, nor hepatic and systemic inflammation.

Glp2r$^{-/-}$ mice exhibit impaired glucose tolerance and enhanced hepatic fat deposition.

Previous studies have demonstrated that both gain and loss of GLP-2 action promoted hepatic steatosis in HFD-fed mice (13, 17). To resolve this discrepancy, we assessed indices of glucose and lipid metabolism in male *Glp2r*$^{-/-}$ and *Glp2r*$^{+/+}$ littermate control mice fed a HFHC or CD for 17 weeks (Figure 3A). HFHC-fed mice exhibited increased weight gain and liver mass; however, these parameters were not different in *Glp2r*$^{-/-}$ mice (Figure 3B, Supplemental Figure 2A). *Glp2r*$^{-/-}$ mice demonstrated elevated AUC glucose during the 2nd hour of intraperitoneal glucose tolerance (Figure 3C). Fasting plasma lipid profiles, including LDL, HDL, total cholesterol and TG were not different in *Glp2r*$^{-/-}$ vs. *Glp2r*$^{+/+}$ mice (Figure 3D,E).

CD-fed *Glp2r*$^{-/-}$ mice exhibited greater hepatic Oil Red O staining (Figure 3F) and hepatic cholesterol and TG content were elevated in HFHC diet-fed mice, with no difference between genotypes. However, hepatic cholesterol and TG levels were increased in CD-fed *Glp2r*$^{-/-}$ vs. *Glp2r*$^{+/+}$ mice, despite similar body weights in both genotypes (Figure 3G and 3B). We next

assessed levels of mRNA transcripts corresponding to genes important for TG and cholesterol uptake and degradation, and de-novo lipogenesis. Although the majority of hepatic mRNA transcript levels were not different between genotypes, levels of *Hmgcr, Cpt1a, Hadhb*, and *Pparg* were increased in *Glp2r*$^{-/-}$ mice (Figure 3H).

To assess extra-hepatic mechanisms that could modify the extent of hepatic lipid deposition in *Glp2r*$^{-/-}$ mice, we studied oral lipid absorption as well as dipeptidyl peptidase-4 (DPP-4) activity and prandial GLP-1 levels in a separate cohort of mice. Plasma DPP-4 activity was not different (Supplemental Figure 2C), whereas fasting GLP-1 levels trended higher in *Glp2r*$^{-/-}$ mice (p=0.07) (Supplemental Figure 2D). Plasma TGs were not different in the fasting state or after olive oil challenge (Supplemental Figure 2E,F); however, plasma GLP-1 levels were higher in *Glp2r*$^{-/-}$ mice after enteral olive oil administration (Supplemental Figure 2G). Accordingly, putative differences in DPP-4 activity and increased GLP-1 levels, which might also reduce postprandial lipemia (18, 19), do not likely contribute to elevated lipid deposition and dysglycemia in CD-fed *Glp2r*$^{-/-}$ mice. Hence, *Glp2r*$^{-/-}$ mice develop dysglycemia and increased hepatic lipid deposition, which could not be attributed to known extra-hepatic aspects of GLP-2R signaling.

Biomarkers of hepatic inflammation are selectively increased in *Glp2r*$^{-/-}$ mice.

Circulating transaminase levels were markedly elevated by diet; however, ALT was further elevated in *Glp2r*$^{-/-}$ mice; aspartate transaminase (AST) levels also trended higher (p=0.054) in *Glp2r*$^{-/-}$ mice (Figure 4A). HFHC diet-fed mice also exhibited increased levels of hepatic cytokines. Notably, levels of TNF-α, IL-6, and KC/GRO were higher in *Glp2r*$^{-/-}$ mice (Figure 4B). Nevertheless, while plasma levels of TNF-α, KC/GRO and IL-10 were increased after HFHC feeding, plasma cytokine levels were not different in *Glp2r*$^{+/+}$ vs *Glp2r*$^{-/-}$ mice (Figure 4C). Similarly, HFHC diet-fed mice exhibited increased hepatic expression of several inflammatory and cellular stress genes (Figure 4D), with mRNA levels for *Crp, Cxcr2*, and *Pkr* higher in *Glp2r*$^{-/-}$ vs. *Glp2r*$^{+/+}$ mice. Interestingly, levels of *Oas2*, an interferon-gamma responsive transcript, were decreased in *Glp2r*$^{-/-}$ liver (Figure 4D).

Hence, *Glp2r*$^{-/-}$ mice exhibit increased hepatic inflammation exemplified by increases in chemokines and interferon-gamma responsive mRNA transcripts.

The *Glp2r* is expressed in hepatic stellate cells (HSC).

To understand how loss of the GLP-2R might predispose to increased hepatic inflammation and lipid deposition, we assessed hepatic *Glp2r* expression. The liver expresses low levels of mRNA transcripts corresponding to a full length GLP-2 receptor (8, 10), previously suggested to be localized to mouse and human hepatocytes (11). We detected expression of full length *GLP2R* mRNA transcripts in 3 commercially available human liver total RNA samples (Figure 5A). The hepatocyte fraction isolated from mouse liver, confirmed by cell-specific marker expression (Supplemental Figure 3A), did not contain *Glp2r* mRNA transcripts, whereas the non-parenchymal (NPC) fraction contained detectable *Glp2r* mRNA transcripts (Figure 5B). Since

hepatic stellate cells (HSC) are not efficiently recovered by standard NPC isolation protocols, we analyzed highly purified hepatic stellate cell fractions (20) (Figure 5C-E). Purity of HSC sorted fractions was confirmed through fluorescent microscopy (Figure 5E) and mRNA abundance of markers for HSC and non-stellate cell fractions (Figure 5D). A substantial enrichment of *Glp2r* expression was observed in highly purified HSCs relative to levels in total liver RNA (Figure 5F), with expression levels in HSCs ~50% of those detected in the jejunum. Conventional RT-PCR followed by Southern blotting identified a full length *Glp2r* mRNA transcript in RNA from mouse liver and stellate cells, as well as in jejunum (Figure 5G). There was no detectable expression of full length *Glp2r* in RNA isolated from hepatocytes (Figure 5G and Supplemental Figure 3C).

To probe whether hepatic NPCs other than stellate cells express the *Glp2r* we used flow cytometry (Supplemental Figure 3B) to sort NPC subpopulations using CD26, CD31 and CD45 surface markers. $CD31^+/CD45^-$ (endothelial cells), $CD45^+/CD31^-$ (subdivided by green autofluorescence properties to Kupffer cells and other hematopoietic cells), and $CD31^-/CD45^-/CD26^+$ (comprised of cholangiocytes and other non-endothelial, non-hematopoietic NPC, with the exception of hepatic stellate cells that are $CD26^-$) were further identified by marker expression. No *Glp2r* was detected in any of these NPC fractions (Supplemental Figure 3B and 3C).

The HSC GLP-2R is directly activated by GLP-2 in vitro

Activation of GLP-2R signaling rapidly induces immediate-early gene (IEG) expression in the intestine as well as in heterologous cells expressing the GLP-2R (21). Exposure of isolated murine HSCs to GLP-2 increased levels of *Egr1*, *Nr4a*, *Rasd1*, and *Phlda1*, consistent with a functional HSC GLP-2R (Figure 5H, Supplemental Figure 4A).

Regulation of hepatic *Glp2r* expression

We next analyzed hepatic *Glp2r* mRNA expression from different groups of mice exposed to various diets. Mice fed a HFHC diet for 17 weeks exhibited ~2-fold increase in hepatic *Glp2r* expression (Supplemental Figure 4B). A similar increase in hepatic *Glp2r* mRNA transcripts was detected in mice after 12 weeks of 45% HFD feeding (Figure 5I), as well as in mice on a methionine-choline deficient (MCD) diet. Notably, mRNA levels of the stellate cell marker *Pdgfrb*, a reflection of HSC abundance, were not different (Figure S4B).

Genotype-dependent differences in HSC mRNA transcripts

We next analyzed levels of mRNA transcripts for 11 genes reported to be upregulated in the context of HSC activation (22-25) in livers from mice fed a MCD diet for 2 weeks. Three of these markers: *Timp1*, *Mmp13* and *Adora2b* were upregulated in whole liver (Supplemental Figure 4C). In a repository of data from hepatocyte single cell RNA (scRNA) sequencing (12), these three markers were expressed at negligible levels in hepatocytes. Thus, we infer that stellate cell activation markers can be informative from analysis of whole liver RNA. Consistent with these findings, we detected increased transcript abundance for stellate cell markers *Pdgfrb*, *Mmp13*, *Timp1* and *Col8a1* after HFHC feeding, with higher levels for *Timp1* and *Col8a1* detected in

livers from vs *Glp2r*$^{-/-}$ vs. *Glp2r*$^{+/+}$ mice (Figure 6A). However, liver fibrosis, quantified by Sirius red staining (Figure 6B), was increased in HFHC-fed mice but not different in *Glp2r*$^{+/+}$ vs *Glp2r*$^{-/-}$ mice, and mRNA levels of the fibrogenic markers *Col1a1* and *Acta2* were comparable in *Glp2r*$^{+/+}$ vs. *Glp2r*$^{-/-}$ mice (Figure 6B). Furthermore, levels of mRNA transcripts for *Col1a1* and *Acta2*, encoding markers of fibrosis, were also increased in hepatic RNA from 50 week old *Glp2r*$^{-/-}$ mice (Figure 6C).

Activation or loss of GLP-2R signaling does not impact the hepatic response to CCl_4

To assess the importance of the GLP-2R in an independent model of hepatic injury, we used the pro-fibrotic agent CCl_4. Wild-type male C57/BL6 mice were treated with i.p CCl_4 every 3 days, for a total of 4 doses (26). Starting two days prior to initiation of CCl_4 treatment and until termination 3 days after the last CCl_4 injection, mice were treated daily with GLP-2 or vehicle (Figure 7A). CCl_4 -treated mice had elevated levels of plasma ALT, increased liver fibrosis (as approximated by Sirius-Red staining), and elevated levels of mRNA transcripts for several HSC activation markers analyzed in whole liver samples and in purified HSC preparations (Figure 7B-E). Nevertheless, GLP-2 treatment had no effect on any of these endpoints, nor on body weight (Figure 7B-E, Supplemental Figure 4D). Unexpectedly, HSC *Glp2r* expression was ~8-fold lower in CCl_4-treated mice (Figure 7E, far right panel). We next studied the consequences of CCl_4 administration in *Glp2r*$^{+/+}$ vs. *Glp2r*$^{-/-}$ male mice (Figure 8A). Plasma ALT, the extent of Sirius-Red staining, and mRNA levels of HSC activation markers in whole liver were generally similar between groups (Figures 8B-E). Interestingly, mRNA levels of *Lox,* frequently induced in early stages of HSC activation (27), were upregulated in HSCs from *Glp2r*$^{-/-}$ mice (Figure 8E).

Discussion

The current studies were prompted in part by questions surrounding the use of the GLP-2 analogue teduglutide in human subjects with intestinal failure at risk for development of PN-associated hepatosteatosis (28), and the conflicting data surrounding the putative actions of GLP-2 in the liver (13, 17, 29). GLP-2 rapidly increases postprandial levels of triglycerides in mice, hamsters and humans (30-32), suggesting that increased substrate availability may contribute to hepatosteatosis in the setting of sustained GLP-2R signaling. Indeed, Taher and colleagues demonstrated increased hepatic lipogenesis in HFD-fed hamsters treated with GLP-2 as well as in RC-fed mice treated with GLP-2 (13). In contrast, treatment of HFD-fed mice with the GLP-2 receptor antagonist GLP-2(3-33) exacerbated hepatic steatosis in HFD-fed mice (17), whereas GLP-2 administration attenuated development of hepatosteatosis in PN-fed rats after small bowel resection (29). Our data, using administration of a degradation-resistant GLP-2R agonist, revealed no compelling effect of GLP-2 receptor activation on hepatic steatosis in wildtype HFHC-fed mice. Collectively, our data are consistent with findings that teduglutide administration produced no change or reduced levels of transaminases and bilirubin in humans with short bowel syndrome (33).

In contrast, we demonstrated that genetic loss of the *Glp2r* increased the extent of hepatic steatosis and upregulated hepatic cytokine expression in mice. These findings are consistent with data from Baldassano (17) and Cani (14) who demonstrated a protective role for GLP-2R signaling in HFD-fed mice and ob/ob mice treated with or without prebiotics and GLP-2 or a GLP-2 receptor antagonist, respectively. Intriguingly, recent evidence links hepatic stellate cell activity to de novo lipogenesis and the development of experimental steatosis (34). Hence, our current findings of hepatosteatosis and increased hepatic inflammation in *Glp2r*$^{-/-}$ mice are consistent with a putative mechanism arising from loss of the HSC GLP-2R, or potential consequences of absent GLP-2R signaling impacting control of gut barrier function, inflammation and hepatic insulin sensitivity (14). The precise mechanisms linking loss of GLP-2R activity to increased hepatic fat accumulation remain uncertain and require additional investigation.

Despite multiple studies examining the roles of GLP-2R in liver biology, the precise cellular localization of the hepatic GLP-2R has remained uncertain. We localized the hepatic GLP-2R to stellate cells, and not, as previously reported (11), in hepatocytes. Intriguingly, GLP-2 infusion rapidly enhances the appearance of circulating TG-rich lipoprotein-associated retinal palmitate (35), establishing a putative link between GLP-2 action, vitamin A bioavailability and subsequent storage in HSCs. Indeed, the HSC GLP-2R was functional, as GLP-2 directly induced a subset of immediate early genes in stellate cells ex vivo, findings consistent with previous studies of GLP-2R signaling ex vivo (36). Notably, relative *Glp2r* expression in purified HSCs approximates levels detected in RNA isolated from the jejunum, a major site of GLP-2R expression (37). Our data are also consistent with the detection of hepatic stellate cell *Glp2r* expression in studies analyzing scRNA data from murine stellate cells (38).

Interestingly, HSC *Glp2r* transcripts were upregulated after exposure to various diets used for experimental induction of hepatic injury, including a 45% high fat diet, a HFHC diet and a MCD diet. These 3 different diets promote hepatic steatosis, however the MCD diet induces a milder degree of steatosis, no weight gain and increased hepatic inflammation and fibrosis (39). Conversely, mice with CCl_4-induced liver injury exhibited a marked reduction in *Glp2r* expression within stellate cells. Collectively, these data show for the first time that *Glp2r* expression is dynamically regulated in the injured liver, and dietary vs. chemical hepatic insults produce divergent regulation of HSC *Glp2r* expression. These observations reveal the importance of interpreting hepatic GLP-2 action in the context of potential changes in expression of the endogenous GLP-2R.

Current concepts linking the gut to stellate cell activation highlight roles for microbial metabolites, including bile acids (40), as well as bacterial cell wall products, exemplified by lipolysaccharide (41), which engage HSCs via distinct receptors and signaling pathways. Notably, bacterial metabolites (42), cell membrane constituents such as LPS (43, 44), as well as bile acids (45), are also potent stimulators of GLP-1 and GLP-2 secretion from enteroendocrine L- cells (46). Our current findings demonstrate that loss of basal GLP-2R signaling is associated with HSC activation in mice with diet-induced hepatic injury. Collectively, these observations expand the concept of a gut-HSC axis through identification of a functional GLP-2R signaling system within HSCs, diversifying the mechanisms through which nutritional stimuli and microbiota may indirectly modulate HSC activity.

Our studies have several limitations. First, we used whole-body *Glp2r*$^{-/-}$ mice with germline loss of the *Glp2r* that may exhibit developmental or functional compensation, such as elevated levels of GLP-1 as shown here. Tissue-specific and conditional inactivation of the *Glp2r* selectively within hepatic stellate cells would further establish the role of the HSC GLP-2R in the phenotypes observed in our studies. Moreover, we studied predominantly younger mice, and stellate cell activation is known to become more prominent with increasing age (47). Additionally, manipulation of central nervous system GLP-2R signaling has been shown to modulate hepatic insulin sensitivity (48), a pathway that was not directly examined in the current studies. Also, we were unable to detect GLP-2R protein within HSCs due to limitations in the sensitivity and specificity of available GLP-2R antisera (7). Nevertheless, our experiments establish the presence of a full-length *Glp2r* mRNA and functional GLP-2R in HSCs, findings with potential importance for understanding how gut-derived signals impact HSC biology in a broader context.

Given the use of teduglutide in human children and adults with short bowel syndrome and hepatosteatosis, taken together with the emerging importance of hepatic stellate cell activation in the pathophysiology of non-alcoholic fatty liver disease, our findings have translational relevance for understanding how the gut, microbiota and microbial metabolites modify stellate cell adaptive responses to nutritional stress, inflammation and hepatic injury.

METHODS

Animal care and genotyping

Mice were housed (2 to 5 mice per cage), under a 12-h light/12h-dark cycle in the Toronto Centre for Phenogenomics (TCP). Experiments were started in mice at 7-9 weeks of age, or older if involving stellate cell isolation, as indicated in Figure legends. Age-matched mice were randomly assigned to experimental groups. All experiments were done in male mice.

Wild-type (WT) C57Bl/6 male mice were purchased from The Jackson Laboratory (Bar Harbor, ME), and *Glp2r*$^{-/-}$ mice, generated in our lab (49) on a C57Bl/6 background were bred at the TCP animal facility. Genotyping was performed by polymerase chain reaction (PCR) on tail DNA as previously described (49).

Mouse diets

All mice were fed a standard rodent chow diet (RC; 18% kcal from fat, 2018 Harlan Teklad, Mississauga, ON) until initiation of experimental diet at age 7-9 weeks. HFHC arm was introduced as follows: Mice were started on two weeks of 45% high-fat diet (HFD; 45% kcal from fat, D12451i, Research Diets, New Brunswick, NJ), then switched to three weeks of 60% HFD (60% kcal fat, Research Diets #D12492), followed by 12 weeks of a high fat, fructose and cholesterol containing diet (HFHC; 40% kcal fat, 20% kcal fructose and 2% cholesterol, Research Diets #D09100301). The appropriate matching control diet (CD; 10% =kcal fat, 0% fructose and 0% cholesterol, Research Diets #D09100304) was administered in parallel to HFHC feeding to control mice.

Rationale for choice of diet: Fructose-containing diets promote hepatic de novo lipogenesis, fat oxidation and modify the effects of a high-fat diet (HFD) on the development of insulin resistance (50).They are also associated with higher degrees of hepatic inflammation and fibrosis (51).

Additional cohorts: Relating to Supplemental Figure 4B and Supplemental Figure 4C:12 week old wild-type C57BL/6 male mice were maintained on a methionine-choline deficient (MCD) or sufficient (MCS) diet for 14 days. (Cedarlane A02082002Bi, A02082003Bi respectively). Relating to Supplemental Figure 4B 8-week old wild-type mice were fed RC or 45% HFD (Research Diets, D12451i) for 12 weeks.

Relating to Figure 5D: age matched *Glp2r*$^{+/+}$ and *Glp2r*$^{-/-}$ mice bred and housed in the TCP animal facility and fed a regular chow diet until age 1 year.

Excluded mice

One mouse from the experiment described in Figures 1+2 on control diet was excluded prior to allocation to GLP-2 treatment due to unexplained extremely poor weight gain.

One mouse from the experiment described in Figures 3+4 from the group Glp2r+/+ HFHC feed was excluded from analyses after repeat validation genotyping after sacrificing revealed *Glp2r* heterozygosity.

GLP-2 Treatment

Mice were injected subcutaneously with 0.2mg/Kg/day of the long acting GLP-2 analogue h[Gly2]GLP-2. Custom synthesized human [Gly2]GLP-2, used for the experiment described in Figures 1 and 2 henceforth referred to as GLP-2, was from Pepceutical Ltd. (Nottingham, UK). Human [Gly2]GLP-2 (Teduglutide), used for the experiment described in Figures 6H, Supplemental Figure 4A and 7 was a gift from Shire Pharmaceuticals Inc.

GLP-2 was administered twice daily at 9am and 5pm for 11 days (for the experiment described in Figure 1+2) or once daily at 9-10am for 14 days (for the experiment described in Figure 7). Control mice were treated with saline in the same volume. GLP-2 doses and length of treatment were based on previous studies describing the intestinotrophic effects.

CCl4 induced liver fibrosis model

Liver injury was induced by intraperitoneal (IP) injections of 0.7 ul/g CCl_4 (Toronto Research Chemicals, C176905), dissolved in mineral oil (Sigma) (52). Injections were administered in 3-day intervals for a total of 4 injections as described in (20). Euthanasia took place 3 days after the last injection.

Blood and tissue collection

Blood was taken via the tail vein during metabolic studies. For isolation of liver fractions mice were anesthetized with Avertin. For other terminal studies, mice were sacrificed by CO2 inhalation, blood was collected via cardiac puncture into heparin-coated (10units/ml) and centrifuged at 14,000g for 10min at 4°C to collect the plasma. Plasma samples were stored at -80°C until further analyses.

Intestines were flushed with PBS and omental fat removed prior to weight and length measurements. Sections were obtained from the proximal jejunum for RNA and protein analyses. Gallbladder volume measurement was performed as described previously (8). Briefly, the gallbladder was ligated to prevent emptying and resected prior to liver manipulation. A photograph of the gallbladder was then taken next to a ruler and volume was calculated as ellipsoid volume, assuming both short diameters to be equal**.** The liver was resected and weighed after removal of gallbladder.

Glucose tolerance test

After a 5-6 hour fast, glucose (1.5 mg/g body wt; Sigma-Aldrich, Oakville, ON) was administered through intraperitoneal injection. A blood sample was drawn from a tail vein at 0, 10, 20, 30, 60, 90, and 120 min after glucose administration, and blood glucose levels were measured using a Glucometer Elite blood glucometer (Bayer, Toronto, ON)

Lipid tolerance test

Regular chow diet-fed *Glp2r*$^{+/+}$and *Glp2r*$^{-/-}$ littermate mice (8-12 weeks old) were gavaged orally with 200 µl of olive oil (Sigma) following a 5-6 hour fast. Tail vein blood samples were collected into heparin-coated capillary tubes: 1) before gavage only for DPP-4 activity, 2) before and 1, 2, and 3 hours post gavage for measurement of triglycerides (TG), and 3) before and 10 minutes after gavage for measurement of active GLP-1. Plasma was prepared from the collected blood samples as described above.

Metabolic measurements

Plasma

For lipid tolerance test (Supplemental Figure 2C-G) Plasma triglycerides (TG) were measured using an enzymatic assay (# 11877771 216 (Roche Diagnostics, Indianapolis, IN) and the calibrator 464-01601 (Wako, Mountain View, CA). Active GLP-1 was measured in plasma using a Mesoscale assay (K150JWC-2). DPP-4 activity was measured in 10 µl of plasma using a fluorometric assay (substrate: 10 mM H-Gly-Pro-AMC HBr (Bachem #I-1225, Torrence, CA); standard: AMC (Bachem #Q-1025, Torrence, CA).

All other analytes in plasma were performed by the Pathology core at The Centre for Phenogenomics. Beckman Coulter AU480 clinical chemistry analyzer which measures analytes in plasma or serum samples using photometry testing, in combination with appropriate reagents (ALT, AST, TG, Cholesterol, LDL, HDL), calibrators (Beckman Coulter Lyophilized Chemistry Calibrator Levels 1 and 2), and quality control materials (Bio-Rad Liquid Assayed Multiqual 1 and 3).

Liver

For determination of triglyceride and cholesterol levels in liver, hepatic lipids were extracted following a protocol adapted from Folch et al. (53). Briefly, frozen liver samples were weighed (~20 mg) and lipids were extracted using a 2:1 chloroform-methanol solution, dried under N_2 and reconstituted in 50 µl of 3:2 tert-butyl alcohol:triton X-100/methyl alcohol (1:1) and quantified with a commercially available enzymatic assay kit (TG kit COBAS 7193130, Cholesterol kit Wako Diagnostics 999-02601).

Measurement of plasma and hepatic cytokine levels

Cytokines were measured in 25 ul of mouse plasma or in 40-70 mg of liver tissue homogenized in 500 ul of ice-cold lysis buffer (50 mM Tris HCl pH 8), 1 mM EDTA, 10% glycerol (wt/vol), 0.02% Brij-35 (wt/vol)). Lysis buffer was supplemented with 1 mM dithiothreitol and protease inhibitor for cytokine assay only. Tissue and plasma (containing 10% TED) levels of cytokines were measured using the MSD V-PLEX Mouse Proinflammatory Panel assay kit (Meso- scale). Cytokine concentrations in tissue were normalized to total protein amount measured by Bradford Assay.

Liver histology

Liver samples were fixed in 10% buffered formalin for 48 h and then transferred into 70% ethanol until processing. For Oil-Red-O staining liver tissue was flash frozen in OCT compound. Samples were paraffin-embedded, sectioned at 4 μm thickness, slide-mounted, and stained with hematoxylin and eosin, picro Sirius-Red stain, or Oil-Red-O using standard protocols. Sections were scanned using the ScanScope CS System (Aperio Tehcnologies, Sausalito, CA) and digital images captured at 10X magnification using ImageScope Software (Aperio Technologies) or an OlyVIA 2.9 system (OLYMPUS). Immunostaining was performed by the Pathology core at The Centre for Phenogenomics.

Tissue fibrosis was analyzed in Sirius-Red-stained samples by red pixel count corresponding to stained collagen using the Aperio Imagescope Positive pixel count program that was calibrated once and applied uniformly to five 10X images from each sample. The percentage of red pixels in total pixel area was determined. Tissue lipids were quantified in a similar manner using Oil-Red-O stained sections. 3-4 images per sample were analyzed using ImageJ software reporting red and total pixel counts.

RNA isolation, cDNA, and qPCR

Tissue samples were dissected, weighed, frozen in liquid-nitrogen, and stored at −80 °C. Frozen tissues were homogenized in Tri Reagent (Molecular Research Center, Cincinnati, ON) using a TissueLyser II system (Qiagen, Germantown, MD), and total RNA was extracted using the manufacturer's protocol. Reverse transcription was performed with RNA treated with DNase I (#EN0521, Thermo- Fisher Scientific, Markham ON, Canada), using random hexamers (#58875) and SuperScript III (#18080-044) from Thermo-Fisher Scientific. The resultant cDNA was used to assess mRNA expression by real-time quantitative PCR (QuantStudio 5 System, Thermo-Fisher Scientific) with TaqMan Fast Advanced Master Mix (#4444557, Thermo-Fisher Scientific) and TaqMan Gene Expression Assays (Thermo-Fisher Scientific). The specific gene expression assays used are listed in Supplementary Table 1. Quantification of transcript levels was performed by the $2^{-\Delta CtT}$ method, and expression levels for each gene were normalized to *Ppia or Actb* (β-actin). RNA extracted from purified HSC was normalized to *Ppia or Pdgfrb.*

***Glp2r* full-length mRNA studies**

Human: The expression of full-length *GLP2R* and *GAPDH* transcripts was assessed by RT-PCR in total RNA from the human colon cancer cell line DLD-1, previously confirmed (54) to stably express the human GLP-2R, and in human liver total RNA purchased from the specified commercial sources. PCR products were analyzed by agarose gel electrophoresis followed by SYBR green staining and by Southern blot analysis using an internal *GLP2R*-specific ^{32}P-labeled oligonucleotide probe. The presence of genomic DNA contamination in samples was monitored, in parallel, with control reactions in which the reverse transcriptase (RT) enzyme was omitted from the reaction mixture (RT-),

Expression of mouse *Glp2r* and *Gapdh* transcripts following a similar protocol was assessed in mouse jejunum (positive control), liver, isolated hepatocytes and purified HSCs.

Human *GLP2R* PCR primer set: forward 5'-TTGTGAAGGTGCACGAGGAA-3' & reverse: 5'-CACCCTAGATCTCACTCTCT-3' amplification for 35 cycles at 60°C annealing temperature. Product size 1,687 bp spanning the entire GLP-2R open reading frame.

Gapdh PCR primer set: forward 5'-GACCACAGTCCATGACATCACT-3' & reverse: 5'-TCCACCACCCTGTTGCTGTAG-3' amplification for 25 cycles at 60°C annealing temperature. Product size 450 bp. This primer set is identical in human and mouse.

Mouse *Glp2r* primer set: forward 5'-GCCCAGTAGATGCAGAGAGG-3' & reverse: 5'-AGTTGCCAAGCTGTGGTGAT-3' amplification for 37 cycles at 60°C annealing temperature. Product size 1,661 bp spanning the entire GLP-2R open reading frame.

Hepatocyte and Hepatic Non-Parenchymal cell isolation

Primary hepatocyte isolation was as previously described (55). For purification of the hepatic non-parenchymal cell (NPC) fraction, the hepatocytes were depleted by 2 minutes centrifugation at 50g, and the supernatant containing NPC cells was isolated and centrifuged for 5 minutes at 300g. The pellet was re-suspended in hepatocyte wash medium (ThermoFisher 17704024). After 4 cycles of hepatocyte depletion, the NPC pellet was enriched in cells expressing macrophage and endothelial cell markers and depleted of albumin- expressing hepatocytes (Supplemental Figure 3A) and was collected for further analysis.

Stellate cell isolation and FACS purification

Isolation of stellate cells from mouse livers was performed following the protocol described in (20). Briefly, the inferior vena cava was cannulated, the portal vein resected, and the superior vena cava clamped. Where appropriate, a segment of the left liver lobe was clamped prior to cannulation and resected for histology and mRNA/protein expression analyses. Following cannulation, the liver was perfused with a series of buffers containing EGTA, pronase and collagenase, removed and mechanically disrupted in pronase+collagenase mix at 37°C. Stellate cells were then isolated by Nycodenz (Alere Technologies, 1002424)-based gradient isolation at 1380*g* at 4°C.

The stellate enriched fraction was removed, stained with the vital dye 7-aminoactinomycin D (7-AAD) (BD Pharmingen 559925) and purified by flow cytometry, performed by the flow cytometry core at The Centre for Phenogenomics using MoFlo Astrios EQ (Beckman Coulter, Miami, FL, USA) equipped with 405nm, 488nm, 561nm, and 640nm lasers and running Summit v.6.2 software. Live stellate cells were identified by the following fluorescent signal combination: low 7-AAD (detector parameter 488-620/29), high 405nm violet laser autofluorescence (detector parameter 405-448/59) and low 488nm blue laser autofluorescence (detector parameter 488-513/26). FACS gates were based on stellate cell autofluorescence in the violet range owing to cell-type specific Vitamin-A laden lipid droplets Additional gating to remove cells based on

autofluorescence in the FITC range enhanced purification from Kupffer cells and other minor contaminants. The post sorting Violet+ FITC- gate was confirmed to be highly enriched for HSC markers and depleted for markers of other hepatic cell populations (Figure 5D). Post sorting HSC viability was sampled frequently by 7-AAD and was reproducibly above 95%.

Flow cytometry for fractionation of hepatic non-parenchymal cell populations

After collection of NPC-enriched fractions, cells were passed through a 40um filter, collected by centrifugation at 300*g*, and re-suspended in hepatocyte wash medium (Invitrogen-Gibco). Following 4 cycles of hepatocyte depletion, the NPC pellet was re-suspended in FACS sorting buffer (EDTA 0.5M, HEPES 25mM and FCS 1% in PBS), incubated for 30 min at 4°C in antibody mixes based on CD-26-PE (Biolegend, 137804) , CD-45-APC (Biolegend, 109814) and CD-31-FITC (Biolegend, 102406), and then washed and sorted. Flow cytometry, performed by the flow cytometry core at The Centre for Phenogenomics using equipment and software as detailed above.

In vitro transcriptional response of immediate early genes (IEG) in stellate cells

Immediate early gene (IEG) expression is activated by the stellate cell purification process (56), as well as by fetal bovine serum (FBS) that is typically added during cell sorting and recovery. Hence, we purified HSCs using standard protocols (20) and, following purification, pelleted the cells at 580g and resuspended them in 1.5ml DMEM + charcoal Dextran (Sigma-Aldrich, C6241) treated bovine serum albumin (Sigma-Aldrich A7030) BSA 1% for 50 minutes at 37°C. Following incubation, samples were divided into 3 equal parts and 10% FBS (positive control), GLP-2 (50nM), or vehicle (PBS, in the same volume as GLP-2) was added. The dose of GLP-2 was based on previously established doses for direct induction of GLP-2R signaling in cells ex vivo (36).

To validate that incubation time sufficiently recovered IEG expression to levels amenable to activation, we tested whether the positive control cells, treated with FBS10% demonstrated expression at least 5% higher than the PBS-treated negative control. For those samples we then analyzed the expression in cells treated with GLP-2 50nM, as fold-change from PBS treated cells from the same batch.

Statistics

Statistical comparisons were made by ANOVA followed by a Tukey post-hoc, 2-way ANOVA followed by a Tukey post-hoc, or by unpaired two-tailed Student's t-test (when only 2 conditions). For in vitro incubation assays where attenuation of IEG during recovery was variable, we compared control and treated samples using a two-tailed ratio paired t-test. P value <0.05 was considered significant. Analysis was done using GraphPad Prism 7 or 8.2. No methods were used to determine whether the data met assumptions of the statistical approach. Statistical parameters can be found in the figure legends.

Study Approval

All experiments involving mice were approved (Animal Use Protocol (AUP) approval number 20-0045H) by the Animal Care and Use Subcommittee at the Toronto Centre for Phenogenomics (TCP) at Mt. Sinai Hospital.

Author Contributions DJD designed the experiments, analyzed the data and wrote the manuscript. SF, LB, BY, DM and EV designed and executed the experiments, analyzed the data and wrote the manuscript.

Acknowledgements

We thank Dr. Payal Shah (LTRI, Mt. Sinai Hospital) for providing liver RNA analyzed from unpublished MCD experiments. SF has received research fellowship funding from Canadian Pediatric Endocrine Group (CPEG) and Pediatric Endocrine Society (PES) and the Hospital for Sick Children. DJD is supported by a Banting and Best Diabetes Centre-Novo Nordisk chair in Incretin Biology. EV was supported by a Diabetes Canada fellowship. These studies were funded in part by operating grant support from CIHR 154321, and Shire-Takeda Pharmaceuticals Inc.

References

1. Drucker DJ. The glucagon-like peptides. *Diabetes.* 1998;47:159-69.
2. Xiao Q, Boushey RP, Drucker DJ, and Brubaker PL. Secretion of the intestinotropic hormone glucagon-like peptide 2 is differentially regulated by nutrients in humans. *Gastroenterology.* 1999;117:99-105.
3. Brubaker PL, Izzo A, Hill M, and Drucker DJ. Intestinal function in mice with small bowel growth induced by glucagon-like peptide-2. *The American journal of physiology.* 1997;272:E1050-E8.
4. Drucker DJ, Ehrlich P, Asa SL, and Brubaker PL. Induction of intestinal epithelial proliferation by glucagon-like peptide 2. *Proc Natl Acad Sci USA.* 1996;93:7911-6.
5. Jeppesen PB, Gilroy R, Pertkiewicz M, Allard JP, Messing B, and O'Keefe SJ. Randomised placebo-controlled trial of teduglutide in reducing parenteral nutrition and/or intravenous fluid requirements in patients with short bowel syndrome. *Gut.* 2011;60(7):902-14.
6. Drucker DJ. The discovery of GLP-2 and development of teduglutide for short bowel syndrome. *ACS Pharmacology and Translational Science.* 2019;March DOI: 10.1021/acsptsci.9b00016.
7. Drucker DJ, and Yusta B. Physiology and pharmacology of the enteroendocrine hormone glucagon-like peptide-2. *Annual review of physiology.* 2014;76:561-83.
8. Yusta B, Matthews D, Flock GB, Ussher JR, Lavoie B, Mawe GM, et al. Glucagon-like peptide-2 promotes gallbladder refilling via a TGR5-independent, GLP-2R-dependent pathway. *Mol Metab.* 2017;6(6):503-11.
9. Gether IM, Nexoe-Larsen C, and Knop FK. New Avenues in the Regulation of Gallbladder Motility-Implications for the Use of Glucagon-Like Peptide-Derived Drugs. *The Journal of clinical endocrinology and metabolism.* 2019;104(7):2463-72.
10. Yusta B, Matthews D, Koehler JA, Pujadas G, Kaur KD, and Drucker DJ. Localization of Glucagon-Like Peptide-2 Receptor Expression in the Mouse. *Endocrinology.* 2019;160(8):1950-63.
11. El-Jamal N, Erdual E, Neunlist M, Koriche D, Dubuquoy C, Maggiotto F, et al. Glugacon-like peptide-2: broad receptor expression, limited therapeutic effect on intestinal inflammation and novel role in liver regeneration. *American journal of physiology Gastrointestinal and liver physiology.* 2014;307(3):G274-85.
12. Halpern KB, Shenhav R, Matcovitch-Natan O, Toth B, Lemze D, Golan M, et al. Single-cell spatial reconstruction reveals global division of labour in the mammalian liver. *Nature.* 2017;542(7641):352-6.
13. Taher J, Baker C, Alvares D, Ijaz L, Hussain M, and Adeli K. GLP-2 Dysregulates Hepatic Lipoprotein Metabolism, Inducing Fatty Liver and VLDL Overproduction in Male Hamsters and Mice. *Endocrinology.* 2018;159(9):3340-50.
14. Cani PD, Possemiers S, Van de Wiele T, Guiot Y, Everard A, Rottier O, et al. Changes in gut microbiota control inflammation in obese mice through a mechanism involving GLP-2-driven improvement of gut permeability. *Gut.* 2009;58(8):1091-103.
15. Buchman AL, Naini BV, and Spilker B. The Differentiation of Intestinal-Failure-Associated Liver Disease from Nonalcoholic Fatty Liver and Nonalcoholic Steatohepatitis. *Semin Liver Dis.* 2017;37(1):33-44.
16. Javid PJ, Oron AP, Duggan CP, Squires RH, Horslen SP, and Pediatric Intestinal Failure C. The extent of intestinal failure-associated liver disease in patients referred for intestinal rehabilitation is associated with increased mortality: an analysis of the Pediatric Intestinal Failure Consortium database. *J Pediatr Surg.* 2018;53(7):1399-402.
17. Baldassano S, Amato A, Rappa F, Cappello F, and Mule F. Influence of endogenous glucagon-like peptide-2 on lipid disorders in mice fed a high-fat diet. *Endocr Res.* 2016;41(4):317-24.

18. Matikainen N, Manttari S, Schweizer A, Ulvestad A, Mills D, Dunning BE, et al. Vildagliptin therapy reduces postprandial intestinal triglyceride-rich lipoprotein particles in patients with type 2 diabetes. *Diabetologia.* 2006;49(9):2049-57.
19. Hsieh J, Longuet C, Baker CL, Qin B, Federico LM, Drucker DJ, et al. The glucagon-like peptide 1 receptor is essential for postprandial lipoprotein synthesis and secretion. *Diabetologia.* 2010;53(3):552-61.
20. Mederacke I, Dapito DH, Affo S, Uchinami H, and Schwabe RF. High-yield and high-purity isolation of hepatic stellate cells from normal and fibrotic mouse livers. *Nat Protoc.* 2015;10(2):305-15.
21. Yusta B, Holland D, Koehler JA, Maziarz M, Estall JL, Higgins R, et al. ErbB signaling is required for the proliferative actions of GLP-2 in the murine gut. *Gastroenterology.* 2009;173(3):986-96.
22. De Minicis S, Seki E, Uchinami H, Kluwe J, Zhang Y, Brenner DA, et al. Gene expression profiles during hepatic stellate cell activation in culture and in vivo. *Gastroenterology.* 2007;132(5):1937-46.
23. Baroni GS, D'Ambrosio L, Curto P, Casini A, Mancini R, Jezequel AM, et al. Interferon gamma decreases hepatic stellate cell activation and extracellular matrix deposition in rat liver fibrosis. *Hepatology.* 1996;23(5):1189-99.
24. Mederacke I, Hsu CC, Troeger JS, Huebener P, Mu X, Dapito DH, et al. Fate tracing reveals hepatic stellate cells as dominant contributors to liver fibrosis independent of its aetiology. *Nature communications.* 2013;4:2823.
25. Kristensen DB, Kawada N, Imamura K, Miyamoto Y, Tateno C, Seki S, et al. Proteome analysis of rat hepatic stellate cells. *Hepatology.* 2000;32(2):268-77.
26. Domenicali M, Caraceni P, Giannone F, Baldassarre M, Lucchetti G, Quarta C, et al. A novel model of CCl4-induced cirrhosis with ascites in the mouse. *J Hepatol.* 2009;51(6):991-9.
27. Perepelyuk M, Terajima M, Wang AY, Georges PC, Janmey PA, Yamauchi M, et al. Hepatic stellate cells and portal fibroblasts are the major cellular sources of collagens and lysyl oxidases in normal liver and early after injury. *American journal of physiology Gastrointestinal and liver physiology.* 2013;304(6):G605-14.
28. Kelly DA. Intestinal failure-associated liver disease: what do we know today? *Gastroenterology.* 2006;130(2 Suppl 1):S70-7.
29. Yano K, Kaji T, Onishi S, Machigashira S, Nagai T, Harumatsu T, et al. Novel effect of glucagon-like peptide-2 for hepatocellular injury in a parenterally fed rat model of short bowel syndrome. *Pediatr Surg Int.* 2019;35(12):1345-51.
30. Meier JJ, Nauck MA, Pott A, Heinze K, Goetze O, Bulut K, et al. Glucagon-like peptide 2 stimulates glucagon secretion, enhances lipid absorption, and inhibits gastric acid secretion in humans. *Gastroenterology.* 2006;130(1):44-54.
31. Hsieh J, Longuet C, Maida A, Bahrami J, Xu E, Baker CL, et al. Glucagon-Like Peptide-2 Increases Intestinal Lipid Absorption and Chylomicron Production via CD36. *Gastroenterology.* 2009;137(3):997-1005.
32. Hsieh J, Trajcevski KE, Farr SL, Baker CL, Lake EJ, Taher J, et al. Glucagon-Like Peptide 2 (GLP-2) Stimulates Postprandial Chylomicron Production and Postabsorptive Release of Intestinal Triglyceride Storage Pools via Induction of Nitric Oxide Signaling in Male Hamsters and Mice. *Endocrinology.* 2015;156(10):3538-47.
33. Schwartz LK, O'Keefe SJ, Fujioka K, Gabe SM, Lamprecht G, Pape UF, et al. Long-Term Teduglutide for the Treatment of Patients With Intestinal Failure Associated With Short Bowel Syndrome. *Clinical and translational gastroenterology.* 2016;7:e142.
34. Choi WM, Kim HH, Kim MH, Cinar R, Yi HS, Eun HS, et al. Glutamate Signaling in Hepatic Stellate Cells Drives Alcoholic Steatosis. *Cell metabolism.* 2019;30(5):877-89 e7.

35. Dash S, Xiao C, Morgantini C, Connelly PW, Patterson BW, and Lewis GF. Glucagon-like peptide-2 regulates release of chylomicrons from the intestine. *Gastroenterology.* 2014;147(6):1275-84 e4.
36. Yusta B, Somwar R, Wang F, Munroe D, Grinstein S, Klip A, et al. Identification of glucagon-like peptide-2 (GLP-2)-activated signaling pathways in baby hamster kidney fibroblasts expressing the rat GLP-2 receptor. *The Journal of biological chemistry.* 1999;274(43):30459-67.
37. Yusta B, Huang L, Munroe D, Wolff G, Fantaske R, Sharma S, et al. Enteroendocrine localization of GLP-2 receptor expression. *Gastroenterology.* 2000;119(3):744-55.
38. Marcher AB, Bendixen SM, Terkelsen MK, Hohmann SS, Hansen MH, Larsen BD, et al. Transcriptional regulation of Hepatic Stellate Cell activation in NASH. *Scientific reports.* 2019;9(1):2324.
39. Machado MV, Michelotti GA, Xie G, Almeida Pereira T, Boursier J, Bohnic B, et al. Mouse models of diet-induced nonalcoholic steatohepatitis reproduce the heterogeneity of the human disease. *PloS one.* 2015;10(5):e0127991.
40. Yoshimoto S, Loo TM, Atarashi K, Kanda H, Sato S, Oyadomari S, et al. Obesity-induced gut microbial metabolite promotes liver cancer through senescence secretome. *Nature.* 2013;499(7456):97-101.
41. Brun P, Castagliuolo I, Pinzani M, Palu G, and Martines D. Exposure to bacterial cell wall products triggers an inflammatory phenotype in hepatic stellate cells. *American journal of physiology Gastrointestinal and liver physiology.* 2005;289(3):G571-8.
42. Chimerel C, Emery E, Summers David K, Keyser U, Gribble Fiona M, and Reimann F. Bacterial Metabolite Indole Modulates Incretin Secretion from Intestinal Enteroendocrine L Cells. *Cell reports.* 2014;9(4):1202-8.
43. Nguyen AT, Mandard S, Dray C, Deckert V, Valet P, Besnard P, et al. Lipopolysaccharides-mediated increase in glucose-stimulated insulin secretion: involvement of the GLP-1 pathway. *Diabetes.* 2014;63(2):471-82.
44. Lebrun LJ, Lenaerts K, Kiers D, Pais de Barros JP, Le Guern N, Plesnik J, et al. Enteroendocrine L Cells Sense LPS after Gut Barrier Injury to Enhance GLP-1 Secretion. *Cell reports.* 2017;21(5):1160-8.
45. Thomas C, Gioiello A, Noriega L, Strehle A, Oury J, Rizzo G, et al. TGR5-mediated bile acid sensing controls glucose homeostasis. *Cell metabolism.* 2009;10(3):167-77.
46. Müller TD, Finan B, Bloom SR, D'Alessio D, Drucker DJ, Flatt PR, et al. Glucagon-like peptide 1 (GLP-1). *Molecular Metabolism.* 2019;30:72-130.
47. Maeso-Diaz R, Ortega-Ribera M, Fernandez-Iglesias A, Hide D, Munoz L, Hessheimer AJ, et al. Effects of aging on liver microcirculatory function and sinusoidal phenotype. *Aging Cell.* 2018;17(6):e12829.
48. Shi X, Zhou F, Li X, Chang B, Li D, Wang Y, et al. Central GLP-2 enhances hepatic insulin sensitivity via activating PI3K signaling in POMC neurons. *Cell metabolism.* 2013;18(1):86-98.
49. Lee S-J, Lee J, Li KK, Holland D, Maughan H, Guttman DS, et al. Disruption of the murine Glp2r impairs Paneth cell function and increases susceptibility to small bowel enteritis. *Endocrinology.* 2012;153(3):1141-51.
50. Softic S, Meyer JG, Wang GX, Gupta MK, Batista TM, Lauritzen H, et al. Dietary Sugars Alter Hepatic Fatty Acid Oxidation via Transcriptional and Post-translational Modifications of Mitochondrial Proteins. *Cell metabolism.* 2019;30(4):735-53 e4.
51. Clapper JR, Hendricks MD, Gu G, Wittmer C, Dolman CS, Herich J, et al. Diet-induced mouse model of fatty liver disease and nonalcoholic steatohepatitis reflecting clinical disease progression and methods of assessment. *American journal of physiology Gastrointestinal and liver physiology.* 2013;305(7):G483-95.

52. Scholten D, Trebicka J, Liedtke C, and Weiskirchen R. The carbon tetrachloride model in mice. *Laboratory animals.* 2015;49(1 Suppl):4-11.
53. Folch J, Lees M, and Sloane Stanley GH. A simple method for the isolation and purification of total lipides from animal tissues. *The Journal of biological chemistry.* 1957;226(1):497-509.
54. Koehler JA, Harper W, Barnard M, Yusta B, and Drucker DJ. Glucagon-like peptide-2 does not modify the growth or survival of murine or human intestinal tumor cells. *Cancer research.* 2008;68:7897-904.
55. Flock G, Baggio LL, Longuet C, and Drucker DJ. Incretin receptors for glucagon-like peptide 1 and glucose-dependent insulinotropic polypeptide are essential for the sustained metabolic actions of vildagliptin in mice. *Diabetes.* 2007;56(12):3006-13.
56. van den Brink SC, Sage F, Vertesy A, Spanjaard B, Peterson-Maduro J, Baron CS, et al. Single-cell sequencing reveals dissociation-induced gene expression in tissue subpopulations. *Nature methods.* 2017;14(10):935-6.

Figure 1 GLP-2 treatment does not alter glucose and lipid metabolism in HFHC diet-fed mice.

(A-H) Metabolic endpoints in mice with diet induced NAFLD treated with GLP-2.

(A) 7-8 week old wild-type male mice were allocated to HFHC or control diet (CD) for 17 weeks, then treated with h[Gly2]GLP-2 (0.1mg/kg BID) or vehicle for the last 11 days on diet (n=9-10 per group for all panels). (B) Body weight gain. (C) Intraperitoneal glucose tolerance in 5-6 hour fasted mice after 5 days of GLP-2 or vehicle. Right panel: area under curve (AUC) 0-120min. (D-E) Plasma lipids at end of study. LDL, Low Density Lipoproteins; HDL, High Density Lipoproteins; TG, triglycerides. (F) Representative Oil-Red-O staining of liver sections (left panel, scale bar 100μm) and quantification of Oil-Red-O-positive staining in liver (right panel). (G) Hepatic cholesterol and TG content. (H) Hepatic mRNA abundance, relative to *Ppia*, of genes relevant to lipid metabolism pathways. Data are presented as the means ± SD. *p<0.05, **p<0.01, ***p<0.001, ****p<0.0001, § significant effect of diet on total variance, p<0.05 using two-way ANOVA with Tukey correction for multiple comparisons.

Figure 2 GLP-2 Treatment in HFHC diet-fed mice does not impact hepatic inflammation.

Experimental endpoints in mice fed a HFHC or CD for 17 weeks and treated with GLP-2 for 11 days as illustrated in Figure 1A. (A) Transaminase plasma levels in cardiac blood at termination. § significant diet effect on ALT variance, p<0.01. (B) Protein concentrations of inflammatory markers in liver normalized to hepatic protein levels. (C) Hepatic mRNA abundance, relative to *Ppia*, of genes relevant to inflammatory pathways. Data are presented as the means ± SD. *p<0.05, **p<0.01, ***p<0.001, § significant effect of diet on gene expression variance, p<0.05 using two-way ANOVA with Tukey correction for multiple comparisons.

Figure 3 *Glp2r*$^{-/-}$ mice exhibit dysglycemia and increased hepatic lipid deposition.

(A-H) Metabolic endpoints in *Glp2r*$^{+/+}$ and *Glp2r*$^{-/-}$ mice fed either a control (CD) or HFHC diet. (A) 7-8 week old *Glp2r*$^{+/+}$ and *Glp2r*$^{-/-}$male mice were allocated to CD or a HFHC diet for 17 weeks (n=9-10/group for all panels). (B) Body weight gain. (C) Intraperitoneal glucose tolerance in 5 hour fasted mice. Right panel: area under curve (AUC) 60-120min. Data are presented as the means ± SD. # Significant effect of genotype on AUC variance, p<0.05 using two-way ANOVA with Tukey correction for multiple comparisons. (D-E) Plasma lipid profiles at endpoint. (F) Representative Oil-Red-O staining of liver sections. Scale bar 100μm. (G) Hepatic cholesterol and triglyceride (TG) content. (H) Hepatic mRNA abundance, relative to *Ppia*, of genes impacting lipid metabolism pathways. Right panels illustrate relative mRNA levels of *Hmgcr, Pparg, Cpt1a,* and *Hadhb* genes for which genotype had a significant effect on gene expression variability. Data are presented as the means ± SD. *p<0.05, **p<0.01, ***p<0.001, § significant effect of diet,

#significant effect of genotype on variance of gene expression, $p<0.05$ using two-way ANOVA with Tukey correction for multiple comparisons.

Figure 4 *Glp2r*$^{-/-}$ mice exhibit enhanced hepatic inflammation on a HFHC diet.

(A-D) Hepatic inflammation and fibrosis endpoints in *Glp2r*$^{+/+}$ or *Glp2r*$^{-/-}$ mice fed HFHC or CD for 17 weeks, as shown in Figure 3A (n=9-10/group for all panels). (A) Plasma transaminase levels from cardiac blood at termination. (B) Protein levels of inflammatory markers in liver normalized to hepatic protein levels. (C) Protein concentrations of inflammatory markers in plasma. (D) Hepatic mRNA abundance, relative to *Ppia*, of genes relevant to inflammatory pathways. Right panels illustrate relative mRNA levels of *Oas2, Pkr, Cxcr2,* and *Crp* genes for which genotype had a significant effect on gene expression variability. Data are presented as the means ± SD. *p<0.05, **p<0.01, ***p<0.001, ****p<0.001, #significant effect of genotype on variance of gene expression, p<0.05 using two-way ANOVA with Tukey correction for multiple comparisons.

Figure 5 The canonical *Glp2r* is expressed in hepatic stellate cells.

(A) The expression of human *GLP2R* and *GAPDH* transcripts was assessed by RT-PCR in total RNA in human livers obtained from 3 indicated commercial sources and in RNA from a human *GLP2R* expressing human colon cancer epithelial cell line (DLD-1) as a positive control. For reverse transcription PCR of *GLP2R* we used primers that amplify a 1.687-kb product encompassing the entire *GLP2R* open reading frame. PCR products were analyzed by agarose gel electrophoresis followed by SYBR green staining (top and bottom panels) or by Southern blot with an internal *GLP2R* ^{32}-P-labeled oligonucleotide (middle panel). RT, reverse transcriptase. (B) Levels of *Glp2r* mRNA, relative to *Ppia*, in whole liver (Liv, n=6), isolated hepatocytes (Hep, n=10), and non-parenchymal liver cells (NPC, n=4). (C) Hepatic stellate cells (HSC; n=3) purified by centrifugation and flow cytometry. (D) mRNA abundance, relative to *Ppia*, of HSC (*Col1a1*, *Pdgfrb*) and non-stellate cell (*Spic*, *Cd11b*) markers in purified HSCs and whole liver. (E) Microscopy image demonstrating lipid vacuole autofluorescence in purified HSC. Scale bar=20um. (F) *Glp2r* mRNA abundance, relative to *Ppia*, in jejunum (Jej), liver (Liv), pellet collected after Nycodenz gradient isolation of HSC (Pel), purified HSC fraction gated by size and positive violet autofluorescence (HSC), cells positive for violet and FITC autofluorescence that correspond to HSCs mixed with contaminant cells (FITC), cells gated negative to violet autofluorescence (Vio-), and cells outside size gate (Size-). (G) Full length mouse *Glp2r* expression in jejunum, whole liver, hepatocytes (Hep) and isolated HSCs. *Glp2r* mRNA transcripts were amplified by reverse transcription PCR with primers that amplify a 1.65-kb product encompassing the entire *Glp2r* open reading frame. PCR products were analyzed by agarose gel electrophoresis followed by SYBR green staining (top and bottom panels). Southern blotting with an internal *Glp2r* ^{32}-P-labeled oligonucleotide (middle panel) was used to detect the PCR product. (H) mRNA abundance, relative to *Ppia*, of immediate early genes used as markers of GLP-2 action in isolated HSCs. Hepatic stellate cells were purified from 18 C57BL/6 WT mice 4-6

months old. Cells, combined from 1-4 mice per data point, were incubated for 20min with either 10% fetal bovine serum (FBS), GLP-2 (50nM), or saline (Veh). Data are presented as the means ± SEM. *p<0.05, **p<0.01 using ratio-paired t-test.

Figure 6 Hepatic stellate cell activation markers are elevated in *Glp2r*$^{-/-}$ mice on HFHC diet and in aged mice.

(A) mRNA abundance, relative to *Ppia*, of hepatic stellate cell activation markers in hepatic RNA from *Glp2r*$^{+/+}$ and *Glp2r*$^{-/-}$ mice on HFHC or CD as outlined in Figure 3A. (B) Representative Sirius Red staining of liver sections with quantification of Sirius Red-positive staining (left panels) and liver mRNA abundance, relative to *Ppia*, of fibrosis markers *Col1a1*and *Acta2* (right panel). (C) mRNA levels, relative to *Ppia*, of stellate cell activation markers in liver from *Glp2r*$^{+/+}$ and *Glp2r*$^{-/-}$ male mice age 50±3.5 weeks old (n=4 each). Data are presented as the means ± SD. *p<0.05, **p<0.01, ***p<0.001, ****p<0.0001, using two-way ANOVA with Tukey correction for multiple comparisons or Student's t-test where appropriate.

Figure 7 GLP-2 treatment does not change CCl_4-mediated liver injury and fibrosis.

(A-E) Fibrosis, liver enzymes, and RNA levels of genes reflecting hepatic stellate cell (HSC) activation in C57BL/6 mice treated with CCl_4 or mineral oil vehicle, together with daily GLP-2 (0.2mg/kg, SC) or vehicle. (A) Mice were pre-treated with once daily GLP-2 or vehicle starting 2 days prior to initiation of CCl_4 treatment. A total of 4 CCl_4 (0.7ml/kg) or vehicle intraperitoneal injections were administered (one every 3 days), then mice were sacrificed 3 days after the last CCl_4 injection. GLP-2 was continued until the final day (n=8-11 per group). (B) Plasma ALT levels at sacrifice. (C) Representative Sirius Red staining of liver sections and quantification of Sirius Red-positive area. (D) mRNA abundance of genes corresponding to markers of fibrosis and stellate cell activation in whole liver, normalized to *Ppia.* (E) mRNA abundance of reporters in purified hepatic stellate cells (HSC), normalized to *Pdgfrb*. Each data point represents cells combined from 1-4 mice. Data are presented as the means ± SD. *p<0.05, **p<0.01, ***p<0.001, § significant effect of treatment on gene expression variance, p<0.05 using two-way ANOVA with Tukey correction for multiple comparisons.

Figure 8 Loss of GLP2R function does not impact CCl_4-mediated liver injury and fibrosis.

(A-E) *Glp2r*$^{+/+}$ or *Glp2r*$^{-/-}$ mice were treated with a total of 4 CCl_4 (0.7ml/kg) intraperitoneal injections (one every 3 days), then sacrificed 3 days after the last CCl_4 injection (n=5/group). (A) Experimental design. (B) Plasma ALT levels in *Glp2r*$^{+/+}$ vs. *Glp2r*$^{-/-}$ mice after completion of CCl_4 course. (C) Representative Sirius Red staining of liver sections and quantification of Sirius Red-positive area. Relative mRNA levels of markers of fibrosis and stellate cell activation after completion of CCl_4 administration in RNA from (D) whole liver normalized to *Ppia*, and (E)

purified hepatic stellate cells (HSC) normalized to *Pdgfrb*. Data are presented as the means ± SD. *p<0.05 using Student's t-test.

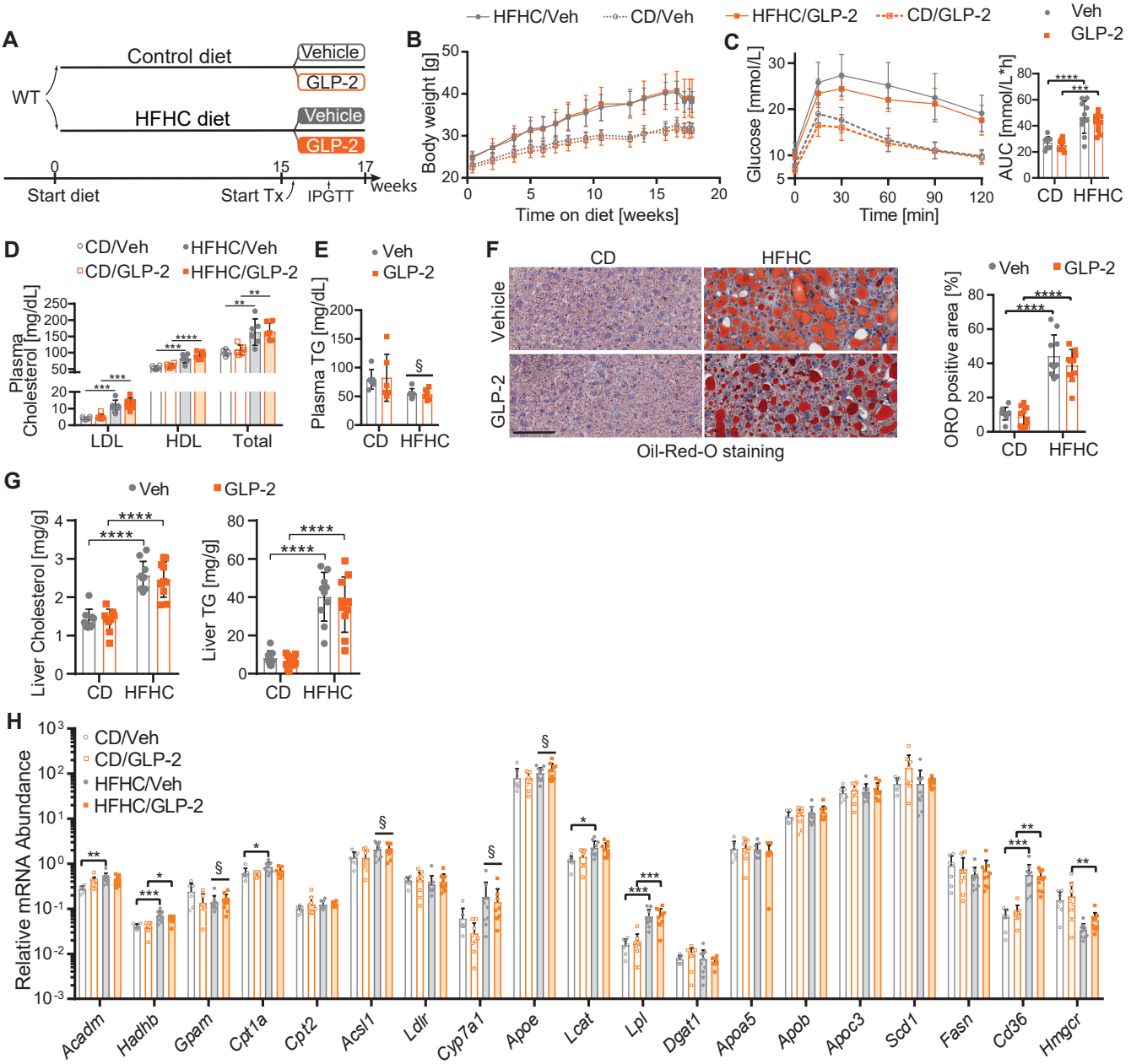

Figure 1 GLP-2 treatment does not alter glucose and lipid metabolism in HFHC diet-fed mice.

(A-H) Metabolic endpoints in mice with diet induced NAFLD treated with GLP-2. (A) 7-8 week old wild-type male mice were allocated to HFHC or control diet (CD) for 17 weeks, then treated with h[Gly2]GLP-2 (0.1mg/kg BID) or vehicle for the last 11 days on diet (n=9-10 per group for all panels). (B) Body weight gain. (C) Intraperitoneal glucose tolerance in 5-6 hour fasted mice after 5 days of GLP-2 or vehicle. Right panel: area under curve (AUC) 0-120min. (D-E) Plasma lipids at end of study. LDL, Low Density Lipoproteins; HDL, High Density Lipoproteins; TG, triglycerides. (F) Representative Oil-Red-O staining of liver sections (left panel, scale bar 100μm) and quantification of Oil-Red-O-positive staining in liver (right panel). (G) Hepatic cholesterol and TG content. (H) Hepatic mRNA abundance, relative to *Ppia*, of genes relevant to lipid metabolism pathways. Data are presented as the means ± SD. *p<0.05, **p<0.01, ***p<0.001, ****p<0.0001, § significant effect of diet on total variance, p<0.05 using two-way ANOVA with Tukey correction for multiple comparisons.

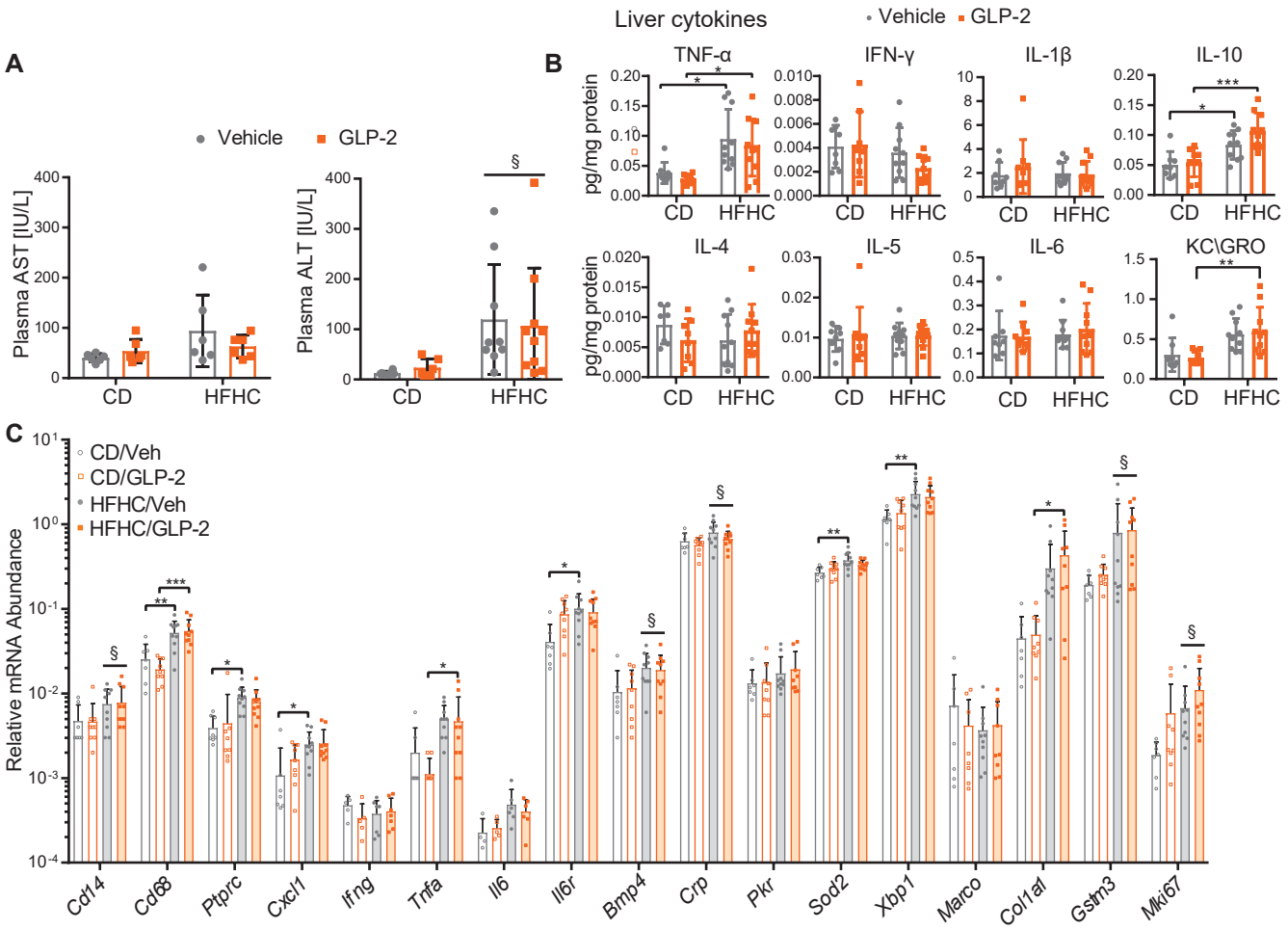

Figure 2 GLP-2 Treatment in HFHC diet-fed mice does not impact hepatic inflammation.

Experimental endpoints in mice fed a HFHC or CD for 17 weeks and treated with GLP-2 for 11 days as illustrated in Figure 1A. (A) Transaminase plasma levels in cardiac blood at termination. § significant diet effect on ALT variance, $p<0.01$. (B) Protein concentrations of inflammatory markers in liver normalized to hepatic protein levels. (C) Hepatic mRNA abundance, relative to *Ppia*, of genes relevant to inflammatory pathways. Data are presented as the means ± SD. *$p<0.05$, **$p<0.01$, ***$p<0.001$, § significant effect of diet on gene expression variance, $p<0.05$ using two-way ANOVA with Tukey correction for multiple comparisons.

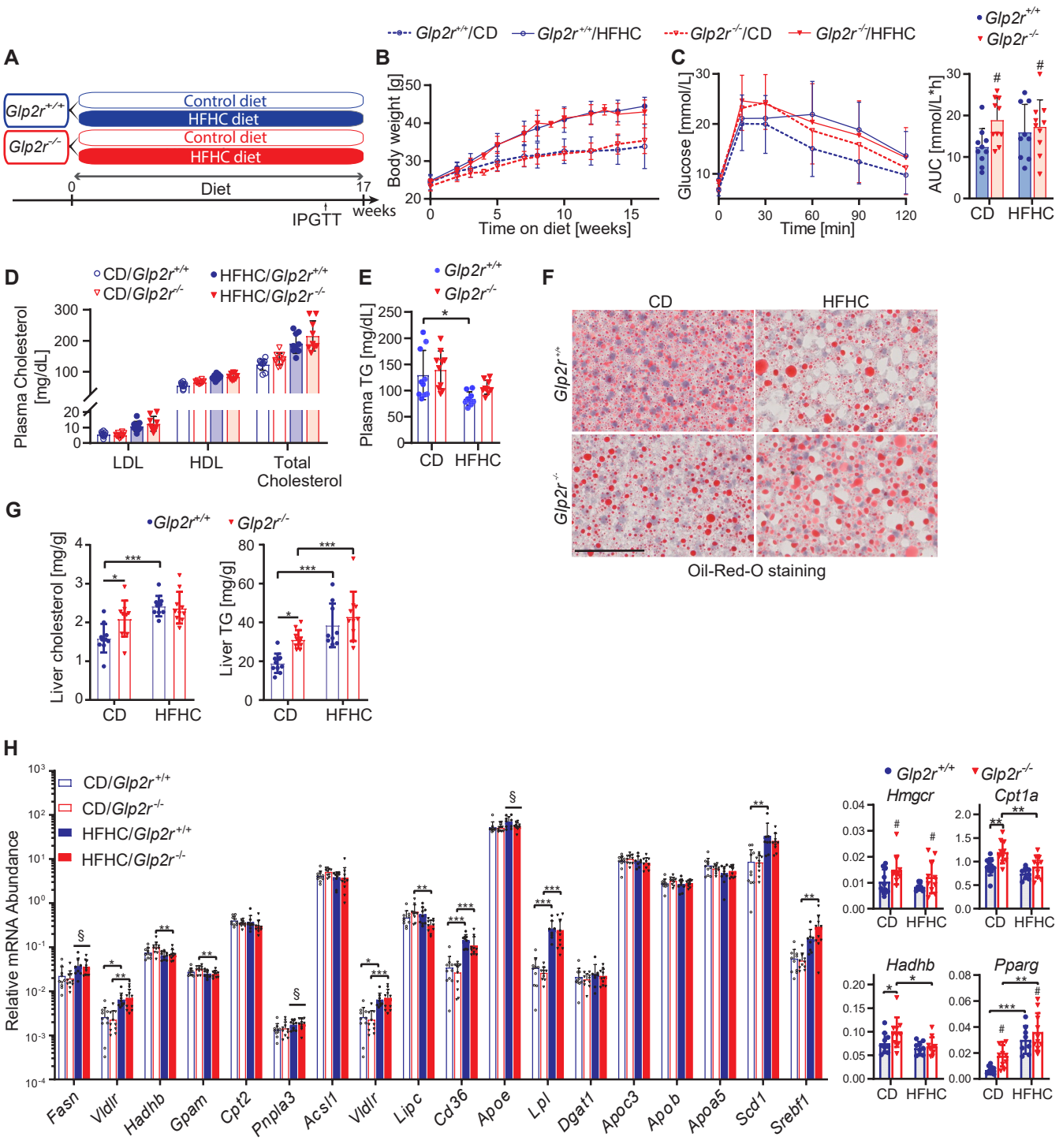
A
Glp2r+/+
Glp2r-/-
Control diet
HFHC diet
Control diet
HFHC diet
0
Diet
17
weeks
IPGTT
B
Glp2r+/+/CD
Glp2r+/+/HFHC
Glp2r-/-/CD
Glp2r-/-/HFHC
Body weight [g]
Time on diet [weeks]
C
Glucose [mmol/L]
Time [min]
AUC [mmol/L*h]
CD
HFHC
D
CD/Glp2r+/+
CD/Glp2r-/-
HFHC/Glp2r+/+
HFHC/Glp2r-/-
Plasma Cholesterol [mg/dL]
LDL
HDL
Total Cholesterol
E
Plasma TG [mg/dL]
F
CD
HFHC
Oil-Red-O staining
G
Liver cholesterol [mg/g]
Liver TG [mg/g]
H
Relative mRNA Abundance
Fasn
Vldlr
Hadhb
Gpam
Cpt2
Pnpla3
Acsl1
Vldlr
Lipc
Cd36
Apoe
Lpl
Dgat1
Apoc3
Apob
Apoa5
Scd1
Srebf1
Hmgcr
Cpt1a
Hadhb
Pparg

Figure 3 *Glp2r*$^{-/-}$ mice exhibit dysglycemia and increased hepatic lipid deposition.

(A-H) Metabolic endpoints in *Glp2r*$^{+/+}$ and *Glp2r*$^{-/-}$ mice fed either a control (CD) or HFHC diet. (A) 7-8 week old *Glp2r*$^{+/+}$ and *Glp2r*$^{-/-}$male mice were allocated to CD or a HFHC diet for 17 weeks (n=9-10/group for all panels). (B) Body weight gain. (C) Intraperitoneal glucose tolerance in 5 hour fasted mice. Right panel: area under curve (AUC) 60-120min. Data are presented as the means ± SD. # Significant effect of genotype on AUC variance, $p<0.05$ using two-way ANOVA with Tukey correction for multiple comparisons. (D-E) Plasma lipid profiles at endpoint. (F) Representative Oil-Red-O staining of liver sections. Scale bar 100µm. (G) Hepatic cholesterol and triglyceride (TG) content. (H) Hepatic mRNA abundance, relative to *Ppia*, of genes impacting lipid metabolism pathways. Right panels illustrate relative mRNA levels of *Hmgcr, Pparg, Cpt1a,* and *Hadhb* genes for which genotype had a significant effect on gene expression variability. Data are presented as the means ± SD. *$p<0.05$, **$p<0.01$, ***$p<0.001$, § significant effect of diet, #significant effect of genotype on variance of gene expression, $p<0.05$ using two-way ANOVA with Tukey correction for multiple comparisons.

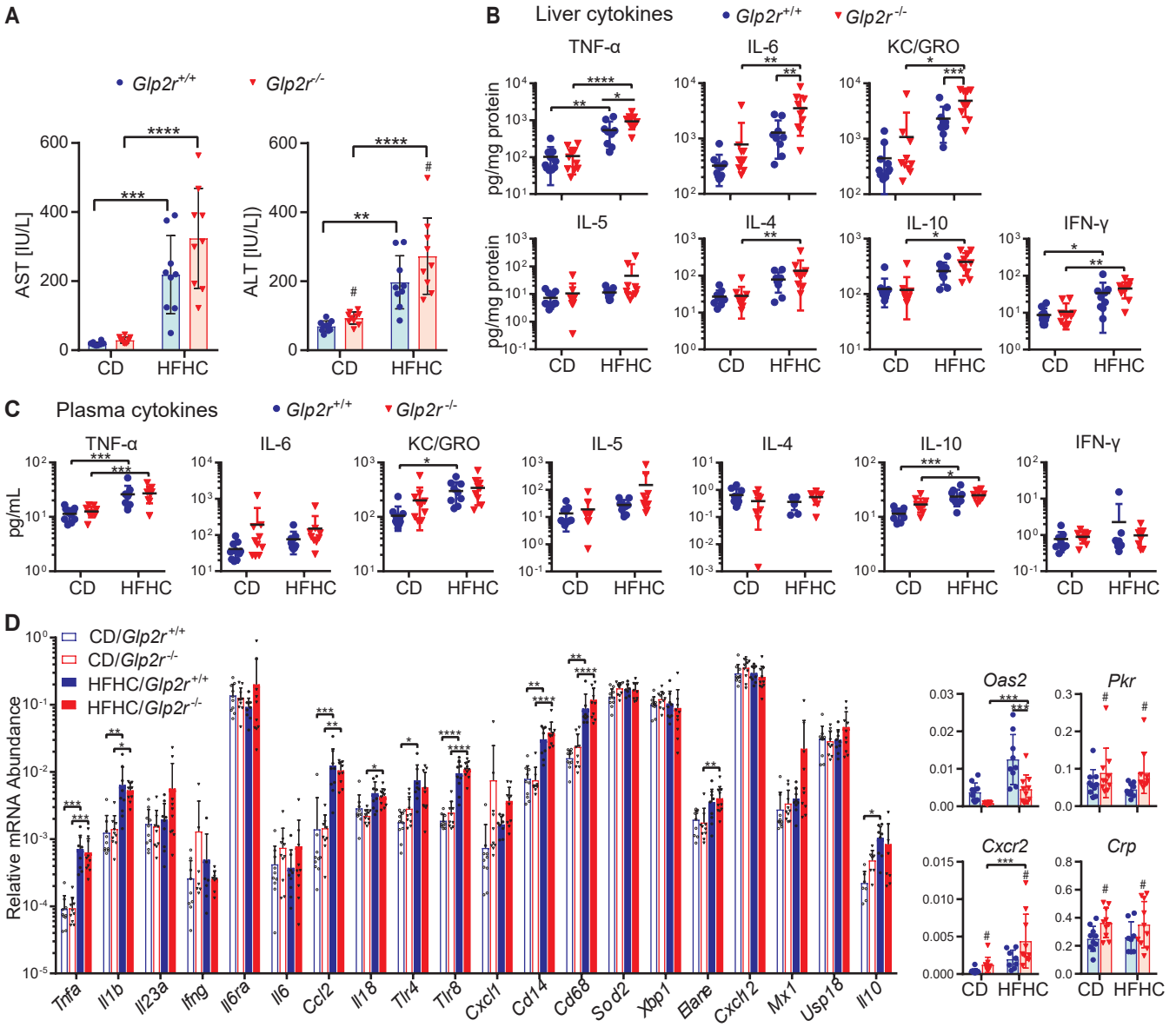

Figure 4 *Glp2r*$^{-/-}$ mice exhibit enhanced hepatic inflammation on a HFHC diet.

(A-D) Hepatic inflammation and fibrosis endpoints in *Glp2r*$^{+/+}$ or *Glp2r*$^{-/-}$ mice fed HFHC or CD for 17 weeks, as shown in Figure 3A (n=9-10/group for all panels). (A) Plasma transaminase levels from cardiac blood at termination. (B) Protein levels of inflammatory markers in liver normalized to hepatic protein levels. (C) Protein concentrations of inflammatory markers in plasma. (D) Hepatic mRNA abundance, relative to *Ppia*, of genes relevant to inflammatory pathways. Right panels illustrate relative mRNA levels of *Oas2, Pkr, Cxcr2,* and *Crp* genes for which genotype had a significant effect on gene expression variability. Data are presented as the means ± SD. *p<0.05, **p<0.01, ***p<0.001, ****p<0.001, #significant effect of genotype on variance of gene expression, p<0.05 using two-way ANOVA with Tukey correction for multiple comparisons.

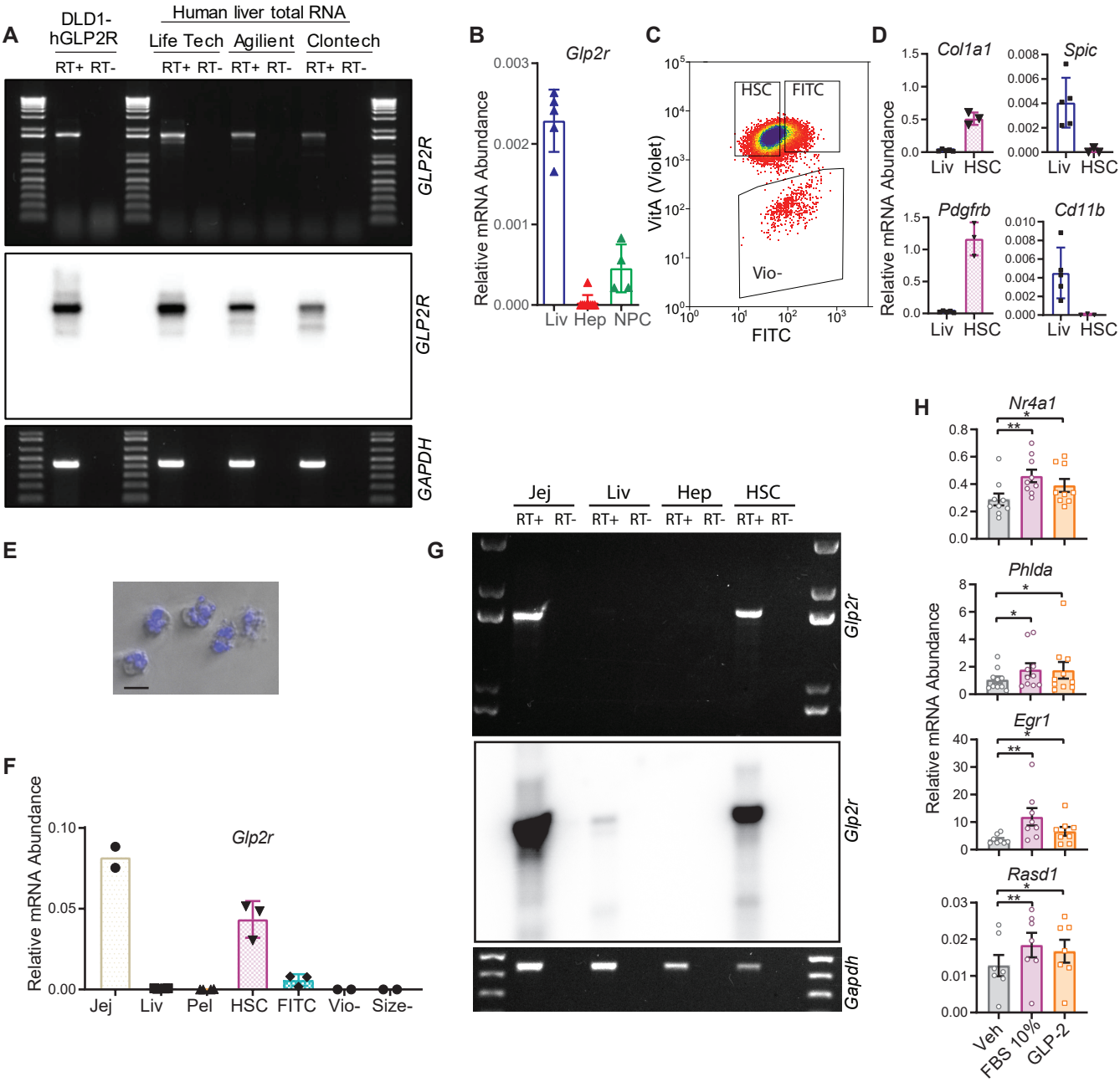
A
DLD1-hGLP2R
Human liver total RNA
Life Tech
Agilient
Clontech
RT+ RT-
GLP2R
GLP2R
GAPDH
B
Glp2r
Relative mRNA Abundance
Liv Hep NPC
C
HSC
FITC
VitA (Violet)
Vio-
FITC
D
Col1a1
Spic
Pdgfrb
Cd11b
Relative mRNA Abundance
Liv HSC
E
F
Glp2r
Relative mRNA Abundance
Jej Liv Pel HSC FITC Vio- Size-
G
Jej Liv Hep HSC
RT+ RT-
Glp2r
Glp2r
Gapdh
H
Nr4a1
Phlda
Egr1
Rasd1
Relative mRNA Abundance
Veh
FBS 10%
GLP-2

Figure 5 The canonical *Glp2r* is expressed in hepatic stellate cells.

(A) The expression of human *GLP2R* and *GAPDH* transcripts was assessed by RT-PCR in total RNA in human livers obtained from 3 indicated commercial sources and in RNA from a human *GLP2R* expressing human colon cancer epithelial cell line (DLD-1) as a positive control. For reverse transcription PCR of *GLP2R* we used primers that amplify a 1.687-kb product encompassing the entire *GLP2R* open reading frame. PCR products were analyzed by agarose gel electrophoresis followed by SYBR green staining (top and bottom panels) or by Southern blot with an internal *GLP2R* ^{32}-P-labeled oligonucleotide (middle panel). RT, reverse transcriptase. (B) Levels of *Glp2r* mRNA, relative to *Ppia*, in whole liver (Liv, n=6), isolated hepatocytes (Hep, n=10), and non-parenchymal liver cells (NPC, n=4). (C) Hepatic stellate cells (HSC; n=3) purified by centrifugation and flow cytometry. (D) mRNA abundance, relative to *Ppia*, of HSC (*Col1a1*, *Pdgfrb*) and non-stellate cell (*Spic*, *Cd11b*) markers in purified HSCs and whole liver. (E) Microscopy image demonstrating lipid vacuole autofluorescence in purified HSC. Scale bar=20um. (F) *Glp2r* mRNA abundance, relative to *Ppia*, in jejunum (Jej), liver (Liv), pellet collected after Nycodenz gradient isolation of HSC (Pel), purified HSC fraction gated by size and positive violet autofluorescence (HSC), cells positive for violet and FITC autofluorescence that correspond to HSCs mixed with contaminant cells (FITC), cells gated negative to violet autofluorescence (Vio-), and cells outside size gate (Size-). (G) Full length mouse *Glp2r* expression in jejunum, whole liver, hepatocytes (Hep) and isolated HSCs. *Glp2r* mRNA transcripts were amplified by reverse transcription PCR with primers that amplify a 1.65-kb product encompassing the entire *Glp2r* open reading frame. PCR products were analyzed by agarose gel electrophoresis followed by SYBR green staining (top and bottom panels). Southern blotting with an internal *Glp2r* ^{32}-P-labeled oligonucleotide (middle panel) was used to detect the PCR product. (H) mRNA abundance, relative to *Ppia*, of immediate early genes used as markers of GLP-2 action in isolated HSCs. Hepatic stellate cells were purified from 18 C57BL/6 WT mice 4-6 months old. Cells, combined from 1-4 mice per data point, were incubated for 20min with either 10% fetal bovine serum (FBS), GLP-2 (50nM), or saline (Veh). Data are presented as the means ± SEM. *$p<0.05$, **$p<0.01$ using ratio-paired t-test.

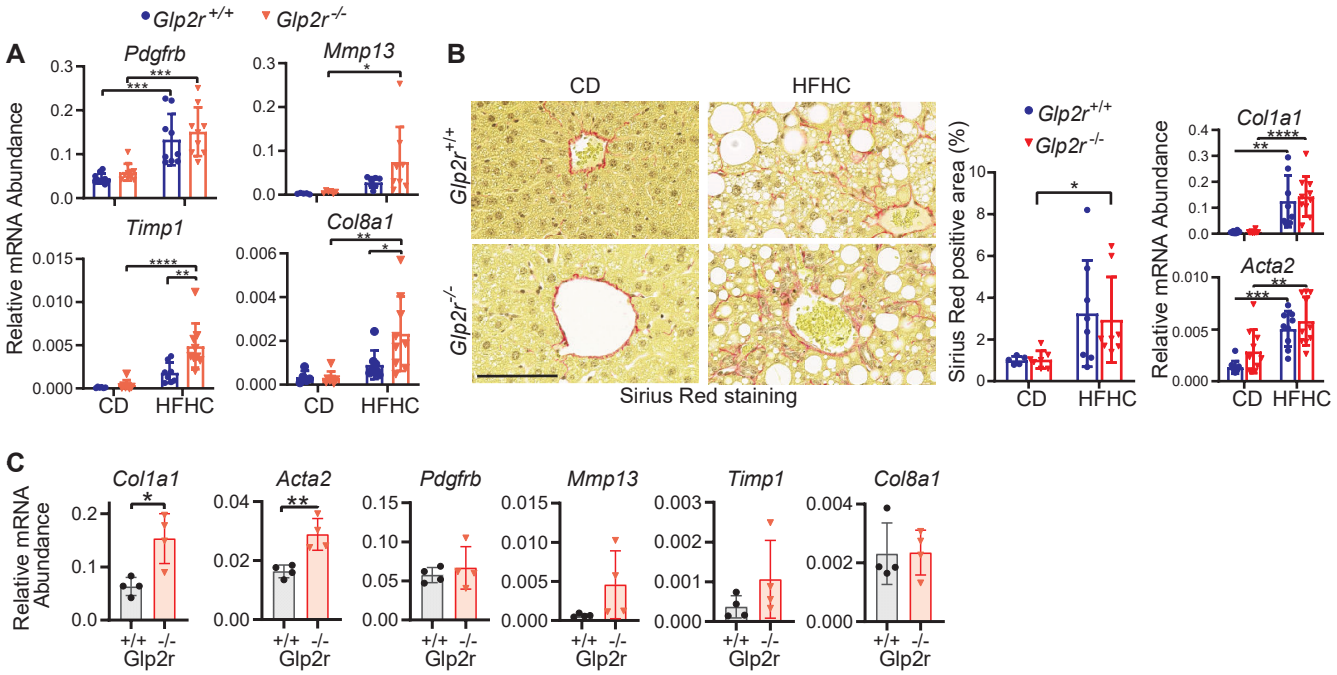

Figure 6 Hepatic stellate cell activation markers are elevated in *Glp2r*$^{-/-}$ mice on HFHC diet and in aged mice.

(A) mRNA abundance, relative to *Ppia*, of hepatic stellate cell activation markers in hepatic RNA from *Glp2r*$^{+/+}$ and *Glp2r*$^{-/-}$ mice on HFHC or CD as outlined in Figure 3A. (B) Representative Sirius Red staining of liver sections with quantification of Sirius Red-positive staining (left panels) and liver mRNA abundance, relative to *Ppia*, of fibrosis markers *Col1a1*and *Acta2* (right panel). (C) mRNA levels, relative to *Ppia*, of stellate cell activation markers in liver from *Glp2r*$^{+/+}$ and *Glp2r*$^{-/-}$ male mice age 50±3.5 weeks old (n=4 each). Data are presented as the means ± SD. *p<0.05, **p<0.01, ***p<0.001, ****p<0.0001, using two-way ANOVA with Tukey correction for multiple comparisons or Student's t-test where appropriate.

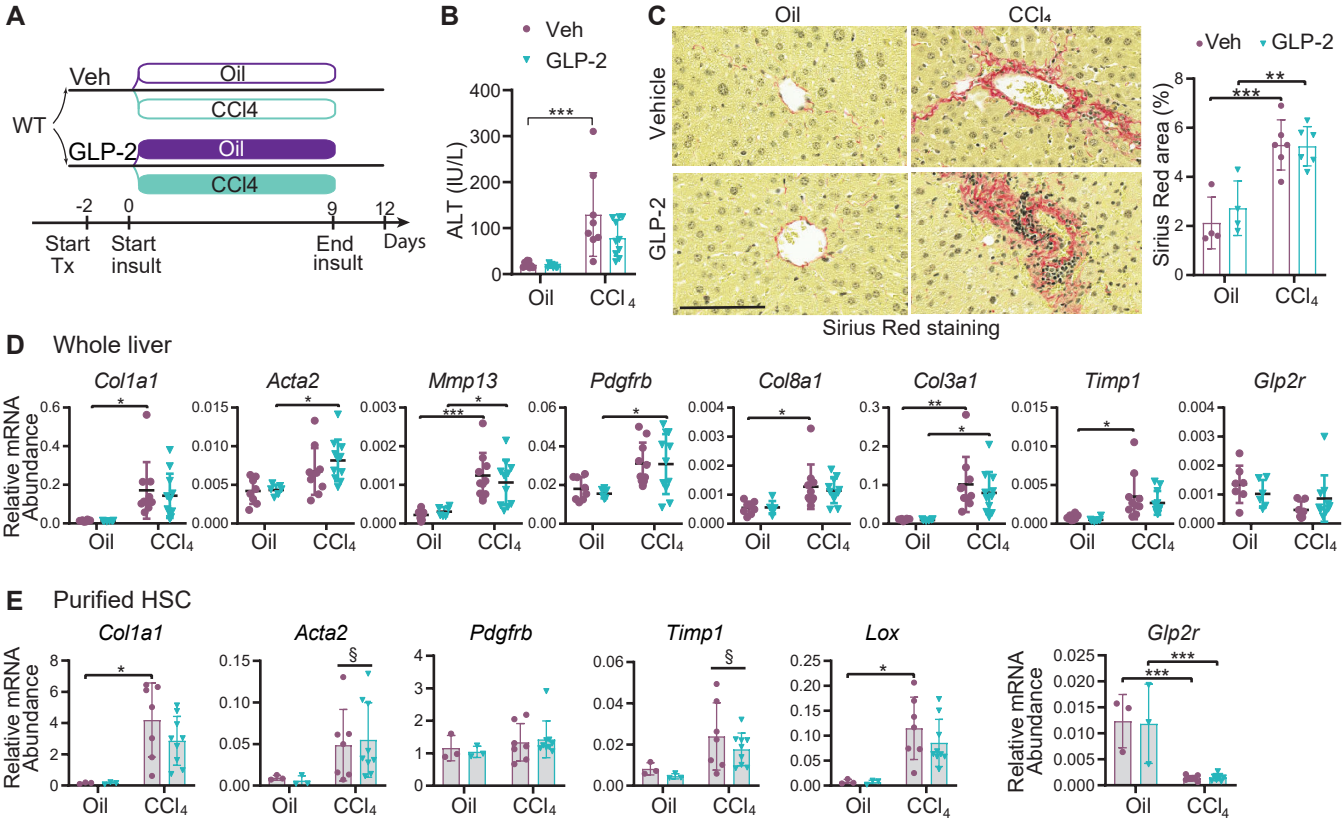

Figure 7 GLP-2 treatment does not change CCl_4-mediated liver injury and fibrosis.

(A-E) Fibrosis, liver enzymes, and RNA levels of genes reflecting hepatic stellate cell (HSC) activation in C57BL/6 mice treated with CCl_4 or mineral oil vehicle, together with daily GLP-2 (0.2mg/kg, SC) or vehicle. (A) Mice were pre-treated with once daily GLP-2 or vehicle starting 2 days prior to initiation of CCl_4 treatment. A total of 4 CCl_4 (0.7ml/kg) or vehicle intraperitoneal injections were administered (one every 3 days), then mice were sacrificed 3 days after the last CCl_4 injection. GLP-2 was continued until the final day (n=8-11 per group). (B) Plasma ALT levels at sacrifice. (C) Representative Sirius Red staining of liver sections and quantification of Sirius Red-positive area. (D) mRNA abundance of genes corresponding to markers of fibrosis and stellate cell activation in whole liver, normalized to *Ppia.* (E) mRNA abundance of reporters in purified hepatic stellate cells (HSC), normalized to *Pdgfrb*. Each data point represents cells combined from 1-4 mice. Data are presented as the means ± SD. *p<0.05, **p<0.01, ***p<0.001, § significant effect of treatment on gene expression variance, p<0.05 using two-way ANOVA with Tukey correction for multiple comparisons.

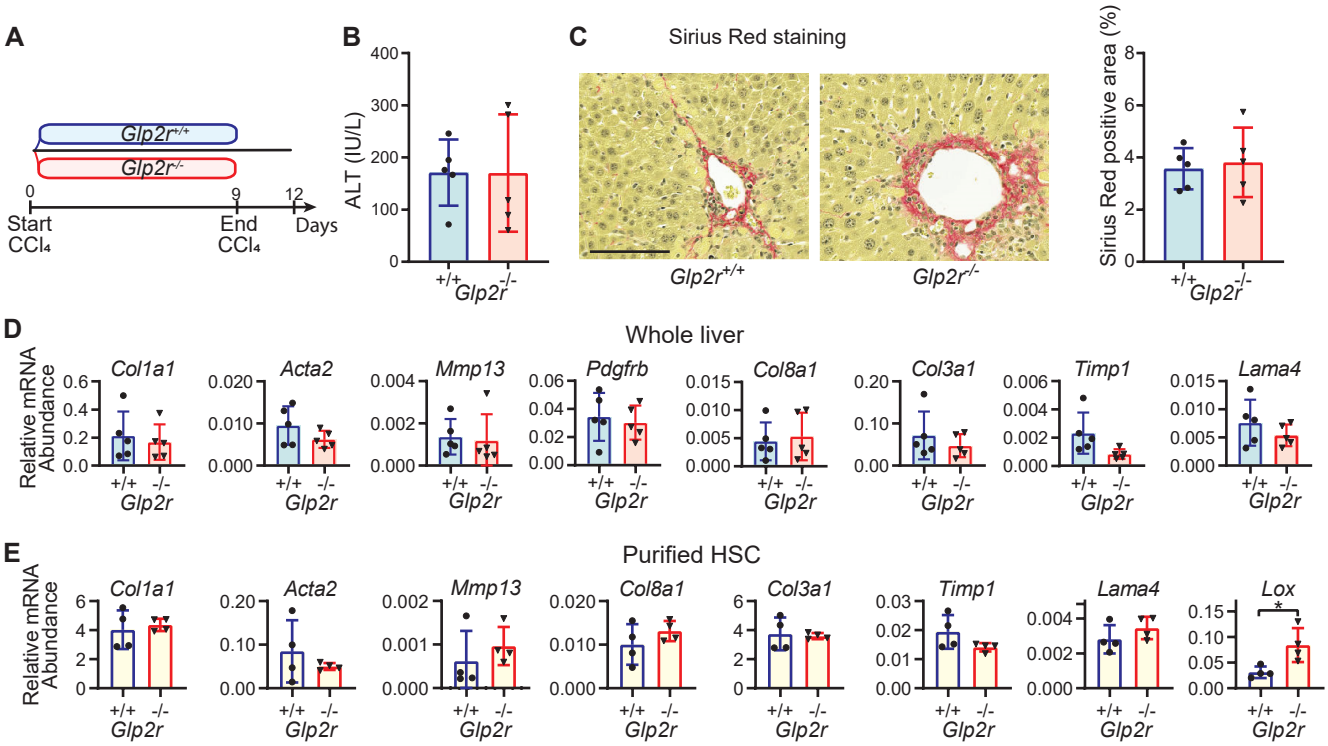

Figure 8 Loss of GLP2R function does not impact CCl_4-mediated liver injury and fibrosis.

(A-E) *Glp2r*$^{+/+}$ or *Glp2r*$^{-/-}$ mice were treated with a total of 4 CCl_4 (0.7ml/kg) intraperitoneal injections (one every 3 days), then sacrificed 3 days after the last CCl_4 injection (n=5/group). (A) Experimental design. (B) Plasma ALT levels in *Glp2r*$^{+/+}$ vs. *Glp2r*$^{-/-}$ mice after completion of CCl_4 course. (C) Representative Sirius Red staining of liver sections and quantification of Sirius Red-positive area. Relative mRNA levels of markers of fibrosis and stellate cell activation after completion of CCl_4 administration in RNA from (D) whole liver normalized to *Ppia*, and (E) purified hepatic stellate cells (HSC) normalized to *Pdgfrb*. Data are presented as the means ± SD. *p<0.05 using Student's t-test.

Supplemental Figures

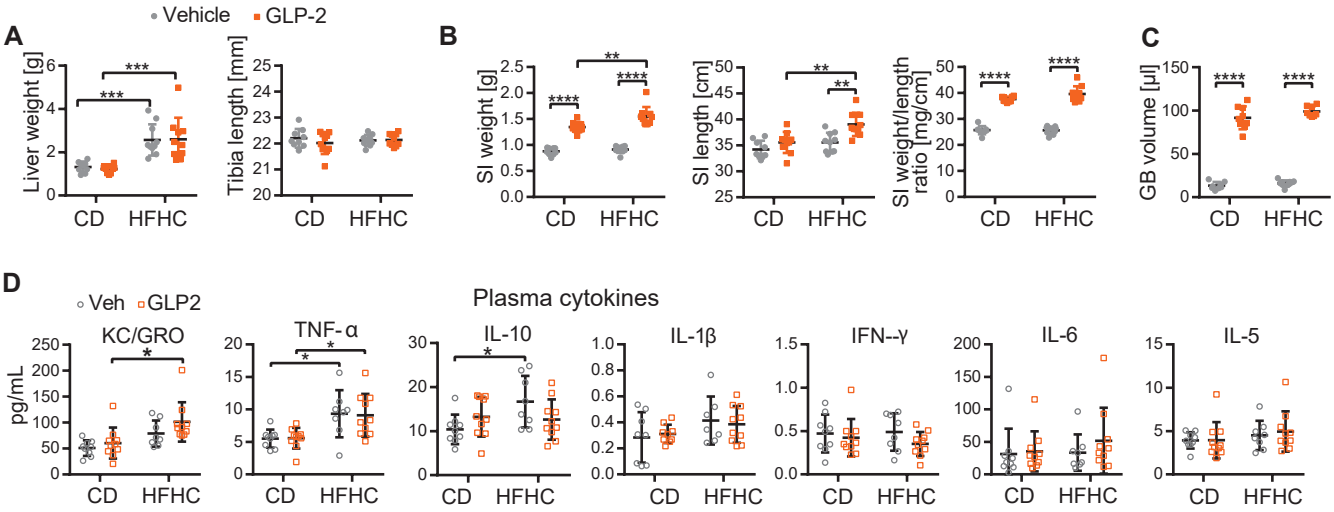

Supplemental Figure S1 Endpoints in mice on HFHC or CD diet treated with GLP-2 or vehicle.

(A) Liver weight (left) and tibia length (right). Tibia length was used for normalization of all measures reported in panels S1A and S1B. (B) Indicators of GLP-2 treatment efficacy: small intestine (SI) weight, length and weight/length ratio. (C) Gallbladder (GB) volume determined by image analysis of GBs that were ligated and resected at termination. (D) Concentrations of inflammatory cytokines in plasma. For (A-D), mice were treated daily with GLP-2 or vehicle for 11 days, with the last dose administered one hour prior to termination, n=9-10 per group. for all panels. Data are presented as the means ± SD. *p<0.05, **p<0.01, ***p<0.001, ****p<0.0001 using two-way ANOVA with Tukey correction for multiple comparisons.

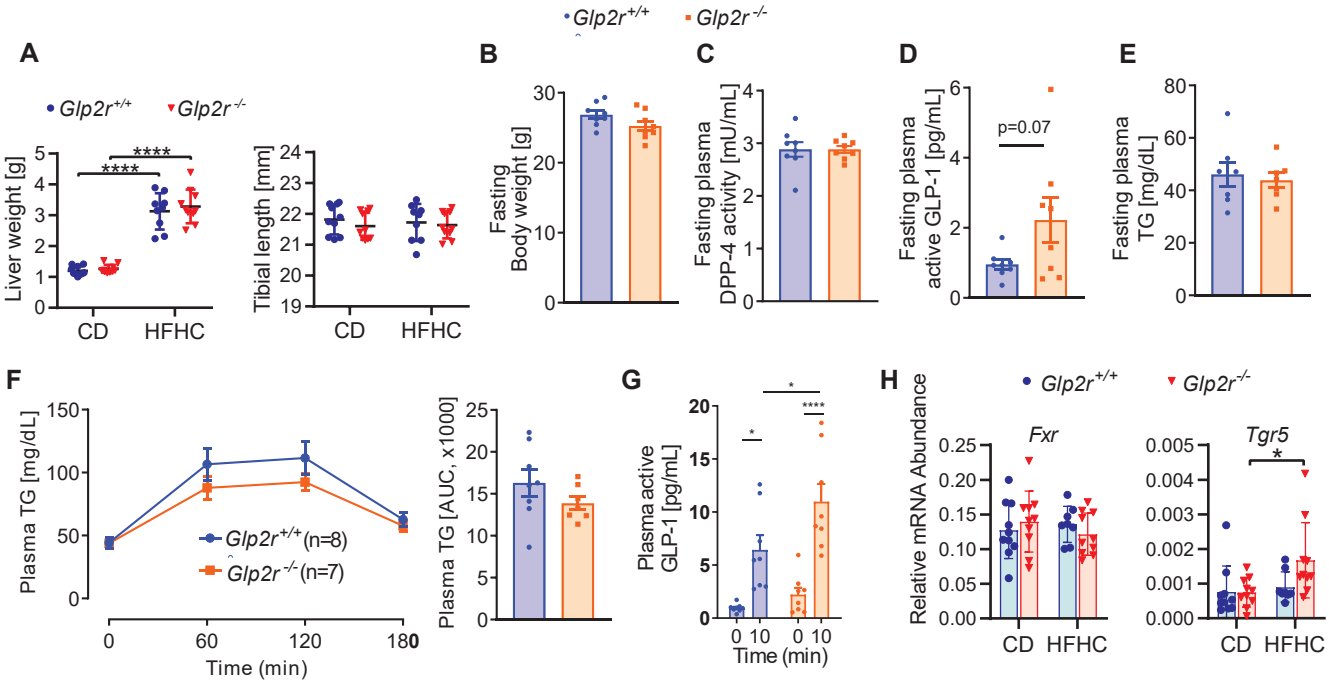

Supplemental Figure S2 Metabolic phenotypes in CD- vs. HFHC-fed mice.

(A) Liver weight (left) normalized to tibia length (right). (B) Body weight. (C) Fasting plasma DPP-4 activity. (D) Fasting plasma active GLP-1 levels. (E) Fasting plasma triglyceride (TG) levels. (F) Plasma TG levels during an oral lipid tolerance test (LTT) and area under curve (AUC) data. (G) Plasma active GLP-1 levels at time 0, and 10min of the LTT in F. Data in (A-G) are from 8-12 week old *Glp2r*$^{+/+}$ and *Glp2r*$^{-/-}$ mice maintained on a RC diet (n=8/group) that were fasted for 5-6 hours prior to analyses. (H) Hepatic mRNA abundance, relative to *Ppia*, of the bile acid sensing receptors *Fxr* and *Tgr5* in *Glp2r*$^{+/+}$ and *Glp2r*$^{-/-}$ mice fed either CD or HFHC diet (n=9-10/group) as described in Figure 3A. Data are presented as the means ± SD. *p<0.05, ****p<0.0001 using two-way ANOVA with Tukey correction for multiple comparisons (panels A,H) or Student's t-test (panels B-G).

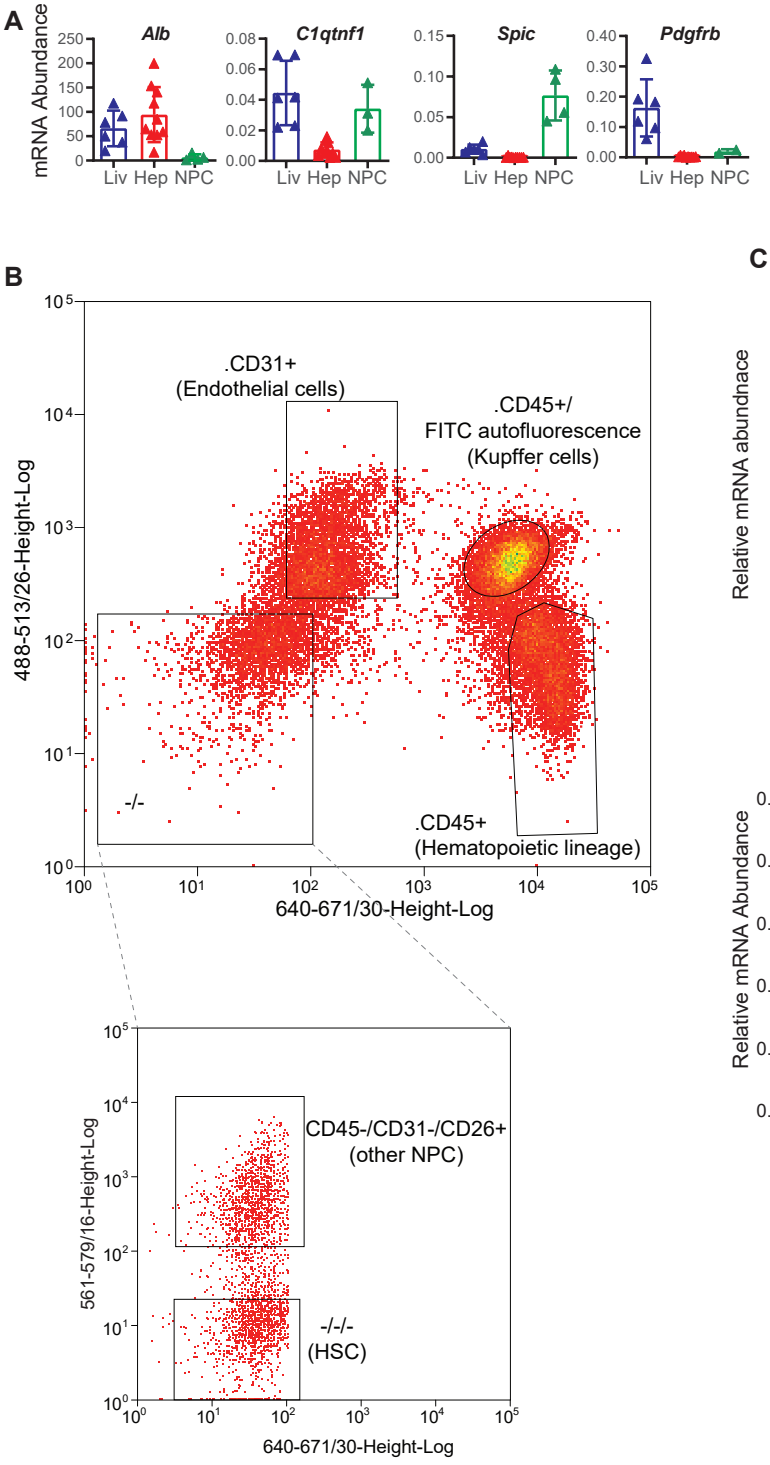

Supplemental Figure S3

Supplemental Figure S3 Fractionation of hepatocytes and non-parenchymal cells (NPC) from whole liver.

(A) mRNA expression of cell type-specific markers in whole liver (Liv, n=6), hepatocyte (Hep, n=10), and non-hepatocyte (NPC, n=4) fractions from male wild-type C57BL/6 mice 8-14 weeks old (n=3 for all panels). (B) Representative scatter plots of NPC fractions from 3 wild-type C57BL/6 male mice, FACS sorted by surface markers enriched for specific subpopulations. Top: $CD31^+$ (endothelial cells); KC $CD45^+$ (hematopoietic lineage cells with autofluorescence in the FITC range, corresponding to Kupffer cells (KC)); CD 45^+ (all other hematopoietic lineage cells); -/- ($CD31^-/CD45^-$ cells). Bottom: $CD31^-/CD45^-$ were further sorted to $CD26^+$ and $CD26^-$ fractions. CD26, also known as dipeptidyl peptidase-4 (DPP4), is expressed in most NPC and absent in HSCs. (C) mRNA abundance of cell-type-specific markers (top panels) and *Glp2r* (bottom panel) in Liv, whole liver; Hep, hepatocytes; Hep $CD26^+$, hepatocytes further purified by sorting to include $CD26^+$ cells; Kupffer, $CD45^+$ gated Kupffer cells from 3 wild-type C57BL/6 male mice. CD31-/CD45-/CD26- fraction corresponding to hepatic stellate cells (HSC) yielded too few cells for mRNA analysis and is not represented. *Cd11b*, hematopoietic marker enriched in both $CD45^+$ and Kupffer gates; *Spic*, Kupffer cell marker; *Cd31*,endothelial marker; *Dpp4*, enriched in hepatocytes and endothelial cells.

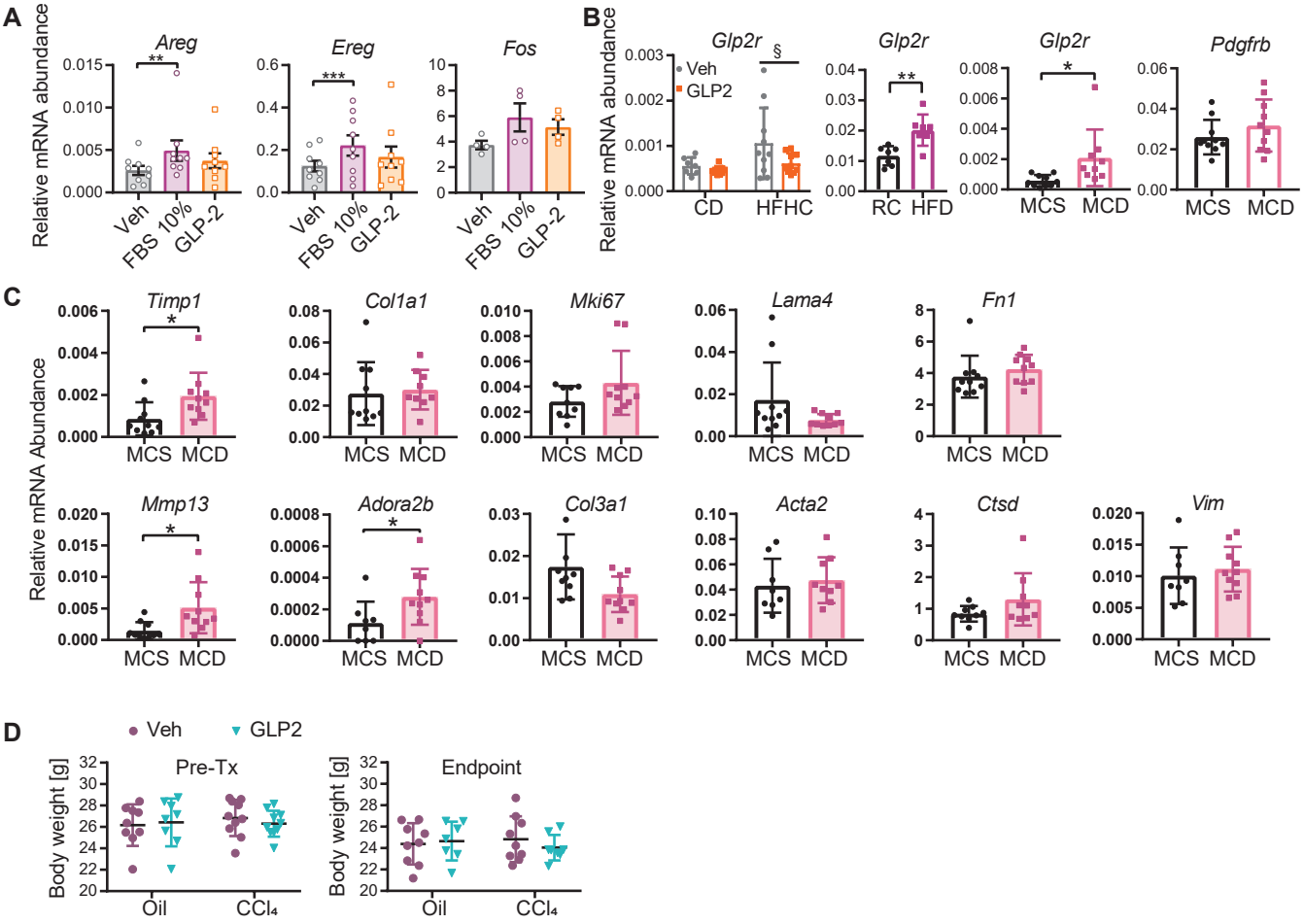

Supplemental Figure S4

(A) mRNA abundance, relative to *Ppia*, of immediate early genes (IEGs) used as markers of GLP-2 action in isolated hepatic stellate cells (HSC, isolated as described in Figures 5C and S3B). As described in Figure 5H, HSC were purified from 18 C57BL/6 WT mice 4-6 months old. Cells, combined from 1-4 mice per data point were incubated for 20min with either 10% fetal bovine serum (FBS), GLP-2 (50nM), or saline (Veh). Data are presented as the means ± SEM. *p<0.05, **p<0.01 using ratio-paired t-test. (B) Glp2r mRNA expression, relative to Ppia, in liver from mice exposed to various diets. From left to right: seventeen weeks of CD or HFHC diet as per Figure 1A (n=9-10/group), 12 weeks of regular chow (RC) or HFD (n=7/group), Glp2r and Pdgfrb (stellate cell marker) expression after 2 weeks of methionine choline sufficient (MCS) or deficient (MCD) diet, bottom panels, (n=9-10/group). Data are presented as the means ± SD. *p<0.05, **p<0.01, ***p<0.001, ****p<0.0001 using two-way ANOVA with Tukey correction for multiple comparisons or Student's t-test where appropriate.(C) mRNA abundance, normalized to *Ppia*, of HSC activation markers in whole liver. Wild-type mice (n=10/diet) were fed a methionine-choline deficient (MCD) or sufficient (MCS) diet for 2 weeks. Data are presented as the means ± SD. *p<0.05 by Student's t-test. (D) Body weights before (Pre-Tx) and at termination (Endpoint) in vehicle (Veh) or GLP-2 treated wild-type mice that received CCl_4 or control (Oil) treatment (n=8-11/group), as described in Figure 7A.

Supplemental Materials and methods

Reagent or resource	Source	Identifier
Chemicals, peptides and recombinant proteins		
Hepatocyte Wash medium	ThermoFisher	17704024
Liver Perfusion Medium	ThermoFisher	17701038
Liver Digest Medium	ThermoFisher	17703034
DNase I grade II	Sigma-Aldrich	10104159001
Pronase	Sigma-Aldrich	P5147
Collagenase D	Sigma-Aldrich (Roche)	11088866001
Tissue-Tek O.C.T compound	Sakura	4583
Mineral oil	Sigma-Aldrich	M1180
Olive oil	Sigma-Aldrich	O1514
Carbon tetrachloride	Toronto research chemicals	C176905
Nycodenz AG	Alere technologies	1002424
7-AAD	BD Pharmingen	559925
DMEM 4.5g/L glucose	Wisent Bioproducts	319-005-CL
Fetal Bovine Serum	Wisenet Bioproducts	080-150
Bovine Serum Albumin (BSA)	Sigma-Aldrich	A7030
Charcoal Dextran	Sigma-Aldrich	C6241
PE anti-mouse CD26 (DPP-4) Ab	Biolegend	137804
APC anti-mouse CD45.2 Ab	Biolegend	109814
FITC anti-mouse CD31 Ab	Biolegend	102406
Teduglutide	Shire Pharmaceutical inc.	7001450

Critical commercial assays		
Mouse Proinflammatory Panel assay kit	Mesoscale	MSD V-PLEX K15048G
Active GLP-1 (ver. 2) kit	Mesoscale	K150JWC-2
Triglyceride assay kit (for plasma TG relating to Figure S2F)	Roche Diagnostics	11877771 216
Triglyceride calibrator (for plasma TG relating to Figure S2F)	Wako	464-01601
H-Gly-Pro-AMC HBr (for DPP-4 activity assay)	Bachem	I-1225
AMC (for DPP-4 activity assay)	Bachem	Q-1025
Protein assay kit II	Biorad	5000002
Triglyceride determination kit (For liver TG content)	**COBAS**	**7193130**
Triglyceride calibrator (For liver TG content)	COBAS	10759350
Cholesterol E kit (For liver cholesterol content)	Wako Diagnostics	999-02601
Experimental models: organisms, strains		
C57BL/6J WT mice	Jackson Laboratories	000664
***Glp2r* Null**	In-house colony at the Toronto Centre for Phenogenomics	Lee, SJ Endocrinology 2012 PMID 2225342

Diets

Regular Chow diet (RC)	Harlan Teklad (Envigo)	2018
10% fat control diet	Research Diets	D09100304
45% high fat diet	Research Diets	D12451i
60% high fat diet	Research Diets	D12492
HFHC diet	Research Diets	D09100301
Methionine-Choline deficient diet (MCD)	Cedarlane	A02082002Bi
Methionine-Choline sufficient diet (MCS)	Cedarlane	A02082003Bi

Software and algorithms

GraphPad Prism, versions 7, 8.3	GraphPad Prism software	https://www.graphpad.com; RRID:SCR_002798
ImageJ	NIH	1.52A
OlyVIA 2.9	OLYMPUS (Build 13735)	www.olympus-sis.com
Aperio ImageScope v12.3.2.8013	Leica Biosystems	https://aperio-imagescope.software.informer.com/12.3/

Others

Human Liver total RNA	Life Tech	AM7960
Human Liver total RNA	Agillient	540017
Human Liver RNA	Clontech	636531
Oligonucleotides		

acetyl-Coenzyme A dehydrogenase, medium chain. (*Acadm*)	Thermo Scientific	Mm00431611_m1
acyl-CoA synthetase long-chain family member 1 (*Acsl1*)	Thermo Scientific	Mm00484217_m1
actin, beta (*Actb*)	Thermo Scientific	Mm00607939_s1
adenosine A2b receptor (*Adora2b*)	Thermo Scientific	Mm00839292_m1
apolipoprotien A5 (*Apoa5*)	Thermo Scientific	Mm00475480_m1
apolipoprotein B (*ApoB*)	Thermo Scientific	Mm01545159_m1
apolipoprotien C3 (*Apoc3*)	Thermo Scientific	Mm00445670_m1
apolipoprotein E (*Apoe*)	Thermo Scientific	Mm00437573_m1
amphiregulin (*Areg*)	Thermo Scientific	Mm00437583_m1
bone morphogenetic protein 4 (*Bmp4*)	Thermo Scientific	Mm00432087_m1
c1q and tumor necrosis factor related protein 1 (*C1qtnf1*)	Thermo Scientific	Mm00480204_m1
chemokine (C-C motif) ligand 2 (*Ccl2*)	Thermo Scientific	Mm00441242_m1
CD14 antigen (Cd14)	Thermo Scientific	Mm00438094_g1
platelet/endothelial cell adhesion molecule 1 (*Pecam1*) (CD31)	Thermo Scientific	Mm01242584_m1
CD36 antigen (*Cd36*)	Thermo Scientific	Mm00432403_m1
CD68 antigen (*Cd68*)	Thermo Scientific	Mm00839636_g1
collagen, type I, alpha 1(*Col1a1*)	Thermo Scientific	Mm00801666_g1
collagen, type III, alpha 1(*Col3a1*)	Thermo Scientific	Mm01254476_m1
collagen, type VIII, alpha	Thermo Scientific	Mm01344184_m1

1(*Col8a1*)		
carnitine palmitoyltransferase 1a, liver (*Cpt1a*)	Thermo Scientific	Mm01231183_m1
carnitine palmitoyltransferase 2 (*Cpt2*)	Thermo Scientific	Mm00487205_m1
C-reactive protein, pentraxin-related (*Crp*)	Thermo Scientific	Mm00432680_g1
cathepsin D (*Ctsd*)	Thermo Scientific	Mm00515586_m1
chemokine (C-X-C motif) ligand 1 (*Cxcl1*)	Thermo Scientific	Mm00433859_m1
chemokine (C-X-C motif) ligand 12 (*Cxcl12*)	Thermo Scientific	Mm00445553_m1
chemokine (C-X-C motif) receptor 2 (*Cxcr2*) (IL8Rb)	Thermo Scientific	Mm00438258_m1
cytochrome P450, family 7, subfamily a, polypeptide 1 (*Cyp7a1*)	Thermo Scientific	Mm00484152_m1
diacylglycerol O-acyltransferase 1 (*Dgat1*)	Thermo Scientific	Mm00515643_m1
dipeptidyl peptidase4 (*Dpp4*)	Thermo Scientific	Mm00494538_m1
early growth response 1 (*Egr1*)	Thermo Scientific	Mm00656724_m1
elastase, neutrophil expressed (*Elane*)	Thermo Scientific	Mm00469310_m1
epiregulin (*Ereg*)	Thermo Scientific	Mm00514794_m1
fatty acid synthase (*Fasn*)	Thermo Scientific	Mm00662319_m1
fibronectin 1 (*Fn1*)	Thermo Scientific	Mm01256744_m1
FBJ osteosarcoma oncogene (Fos)	Thermo Scientific	Mm00487425_m1
nuclear receptor subfamily 1, group H, member 4 (BAR) (FXR)	Thermo Scientific	Mm01240553_m1

(*Nr1h4*)		
glucagon-like peptide 2 receptor (*Glp2r*) Mm01329475_m1	Thermo Scientific	Mm01329475_m1
glycerol-3-phosphate acyltransferase, mitochondrial. (*Gpam*)	Thermo Scientific	Mm00833328_m1
glutathione S-transferase, mu 3 (*Gstm3*)	Thermo Scientific	Mm00833923_m1
hydroxyacyl-Coenzyme A dehydrogenase/3-ketoacyl-Coenzyme A thiolase/enoyl-Coenzyme A hydratase (trifunctional protein), beta subunit (*Hadhb*)	Thermo Scientific	Mm00523880_m1
3-hydroxy-3-methylglutaryl-Coenzyme A reductase (*Hmgcr*)	Thermo Scientific	Mm01282499_m1
interferon gamma (*Ifng*)	Thermo Scientific	Mm01168134_m1
interleukin 10 (*Il10*)	Thermo Scientific	Mm99999062_m1
interleukin 18 (*Il18*)	Thermo Scientific	Mm00434226_m1
interleukin 1 beta (*Il1b*)	Thermo Scientific	Mm01336189_m1
interleukin 23, alpha subunit p19 (*Il23a*)	Thermo Scientific	Mm01160011_g1
interleukin 6 (*Il6*)	Thermo Scientific	Mm00446190_m1
interleukin 6 receptor, alpha (*Il6ra*)	Thermo Scientific	Mm00439653_m1
laminin, alpha 4 (*Lama4*)	Thermo Scientific	Mm01193660_m1
lecithin cholesterol acyltransferase (*Lcat*)	Thermo Scientific	Mm01247340_m1
low density lipoprotein receptor	Thermo Scientific	Mm00440169_m1

(*Ldlr*)		
lipase, hepatic (*Lipc*)	Thermo Scientific	Mm00433975_m1
lysyl oxidase (*Lox*)	Thermo Scientific	Mm00495386_m1
lipoprotein lipase (*Lpl*)	Thermo Scientific	Mm00434770_m1
macrophage receptor with collagenous structure (*Marco*)	Thermo Scientific	Mm00440265_m1
antigen identified by monoclonal antibody Ki 67 (*Mki67*)	Thermo Scientific	Mm01278617_m1
matrix metallopeptidase 13 (*MmP13*)	Thermo Scientific	Mm00439491_m1
MX dynamin-like GTPase 1 (*Mx1*)	Thermo Scientific	Mm00487796_m1
nuclear receptor subfamily 4, group A, member 1 (*Nr4a1*)	Thermo Scientific	Mm01300401_m1
2'-5' oligoadenylate synthetase 2 (Oas2)	Thermo Scientific	Mm00460961_m1
platelet derived growth factor receptor, beta polypeptide (*Pdgfrb*)	Thermo Scientific	Mm00435546_m1
pleckstrin homology-like domain, family A, member 1 (*Phlda1*)	Thermo Scientific	Mm00456345_g1
eukaryotic translation initiation factor 2-alpha kinase 2 PKR (*Eif2ak2*)	Thermo Scientific	Mm01235643_m1
patatin-like phospholipase domain containing 3 (*Pnpla3*)	Thermo Scientific	Mm00504420_m1
peroxisome proliferator activator receptor gamma (*Pparg*)	Thermo Scientific	Mm01184322_m1
Cyclophilin (*Ppia*)	Thermo Scientific	Mm02342430_g1
protein tyrosine phosphatase,	Thermo Scientific	Mm01293577_m1

receptor type, C (*Ptprc*) (CD45)		
RAS, dexamethasone-induced 1 (*Rasd1*)	Thermo Scientific	Mm00842185_g1
stearoyl-Coenzyme A desaturase 1 (*Scd1*)	Thermo Scientific	Mm00772290_m1
superoxide dismutase 2, mitochondrial (*Sod2*)	Thermo Scientific	Mm00449726_m1
Spi-C transcription factor (*Spic*)	Thermo Scientific	Mm00488428_m1
sterol regulatory element binding transcription factor 1 (*Srebp1c, Srebf1*)	Thermo Scientific	Mm00550338_m1
G protein-coupled bile acid receptor 1 (*Tgr5*) (GPBAR1)*	Thermo Scientific	Mm04212121_s1
tissue inhibitor of metalloproteinase 1 (*Timp1*)	Thermo Scientific	Mm00441818_m1
toll-like receptor4 (*Tlr4*)	Thermo Scientific	Mm00445273_m1
toll-like receptor8 (*Tlr8*)	Thermo Scientific	Mm04209873_m1
Tumor necrosis factor alpha (*Tnfa*)	Thermo Scientific	Mm00443258_m1
ubiquitin specific peptidase 18 (*Usp18*)	Thermo Scientific	Mm01188805_m1
vimentin (*Vim*)	Thermo Scientific	Mm01333430_m1
very low density lipoprotein receptor (*Vldlr*)	Thermo Scientific	Mm00443298_m1
X-box binding protein 1 (*Xbp1*)	Thermo Scientific	Mm00457357_m1

CONTACT FOR REAGENT AND RESOURCE SHARING

Further information and requests for resources and reagents should be directed to the Lead Contact, Dr. Daniel J. Drucker (drucker@lunenfeld.ca).